Parameter extraction methods for metamaterials with negative refractive index

João Fernando Corsini

Parameter extraction methods for metamaterials with negative refractive index

João Fernando Corsini

Orientador: **Prof. Dr. Ben-Hur Viana Borges**

Trabalho de Conclusão de Curso submetida à *Escola de Engenharia de São Carlos* – EESC-USP, como uma das disciplinas necessárias para a formação acadêmica em Engenharia Elétrica com Ênfase em Eletrônica.

USP – São Carlos
October 2016

Corsini, João Fernando
C826p Parameter extraction methods for metamaterials with negative refractive index / João Fernando Corsini; orientador Ben-Hur Viana Borges. São Carlos, 2016.

Monografia (Graduação em Engenharia Elétrica com ênfase em Eletrônica) -- Escola de Engenharia de São Carlos da Universidade de São Paulo, 2016.

1. metamaterial. 2. índice de refração negativo. 3. extração dos parâmetros eletromagnéticos. I. Título.

FOLHA DE APROVAÇÃO

Nome: João Fernando Corsini

Título: "Parameter extraction methods for metamaterials with negative refractive index"

Trabalho de Conclusão de Curso defendido e aprovado em 22 / 11 / 2016,

com NOTA 8,8 (oito , oito), pela Comissão Julgadora:

Prof. Associado Ben-Hur Viana Borges - Orientador - SEL/EESC/USP

Prof. Dr. João Paulo Pereira do Carmo - SEL/EESC/USP

Mestre Achiles Fontana da Mota - Doutorando/SEL/EESC/USP

Coordenador da CoC-Engenharia Elétrica - EESC/USP:
Prof. Associado José Carlos de Melo Vieira Júnior

Dedico esse trabalho à minha mãe, pai e irmã por sempre apoiarem minhas decisões.

ACKNOWLEDGEMENTS

First I would like to thank my adviser Dr. Ben-Hur for all his insightful advice and for providing me with everything necessary to prepare this thesis.

I would also like to thank Achiles Fontana for always being helpful whenever I approached him with questions and doubts.

I thank Fanny for helping me to review this whole thesis and being so patience at difficult times.

And finally, I would like to thank all my friends from Torre de Babel. These years wouldn't be the same without you!

“When you talk, you are only repeating what you already know.
But if you listen, you may learn something new.”
J. P. McEvoy

RESUMO

CORSINI, J. F.. **Parameter extraction methods for metamaterials with negative refractive index**. 2016. 46 f. Trabalho de Conclusão de Curso (Engenharia Elétrica com Ênfase em Eletrônica) – Escola de Engenharia de São Carlos (EESC/USP), São Carlos – SP.

Por meio do estudo dos parâmetros eletromagnéticos, este trabalho identifica o que é necessário para se construir um metamaterial com índice de refração negativo e mostra suas diversas aplicações. Utilizando o método de Nicolson-Ross-Weir, a permissividade ε e a permeabilidade μ são derivadas em função dos parâmetros de espalhamento. Então, utilizando técnicas de fabricação de circuito impresso (PCB), duas geometrias diferentes de células são fabricadas em laboratório e medidas. Os resultados obtidos por meio das medidas são então comparados com os simulados, mostrando que é possível obter índice de refração negativo dentro de um guia de ondas ou no espaço livre.

Palavras-chave: metamaterial, índice de refração negativo, extração das parâmetros eletromagnéticas.

ABSTRACT

CORSINI, J. F.. **Parameter extraction methods for metamaterials with negative refractive index**. 2016. 46 f. Trabalho de Conclusão de Curso (Engenharia Elétrica com Ênfase em Eletrônica) – Escola de Engenharia de São Carlos (EESC/USP), São Carlos – SP.

My means of the study of electromagnetic parameters, this work identifies what is necessary to fabricate a metamaterial with negative index of refraction and discuss different applications. Using the Nicolson-Ross-Weir method, the permittivity ε and the permeability μ are derived as a function of the scattering parameters. Then, with printed circuit board (PCB) techniques, two different geometries of cells are fabricated and measured in the lab. The results obtained through measurements are then compared with the simulated ones, showing that it is possible to obtain such properties either inside a waveguide, or in free space.

Key-words: metamaterial, negative index of refraction, extraction of electromagnetic parameters.

LIST OF FIGURES

LIST OF TABLES

LIST OF ABBREVIATIONS AND ACRONYMS

DUT ..... Device under test
HFSS .... High Frequency Structural Simulator
LPI ..... Lines per Inch
MC ..... Perfect Magnetic Conductor
MTM .... Metamaterials
NRW ..... Nicolson–Ross–Weir
PCB ..... Printed Circuit Board
PCB ..... printed circuit board
PEC ..... Perfect Electric Conductor
RHM ..... Right-Hand Material
SRR ..... Split Ring Resonator

LIST OF SYMBOLS

j — Imaginary unit $\sqrt{-1}$

λ — Wavelength

ε — Permittivity

μ — Permeability

n — Index of Refraction

Z — Impedance

ε_0 — Permittivity of vacuum

μ_0 — Permeability of vacuum

ε_r — Relative permittivity of material

μ_r — Relative permeability of material

ε_{eff} — Effective permittivity of material

μ_{eff} — Effective permeability of material

CONTENTS

CHAPTER

1

INTRODUCTION

1.1 Objective

Electromagnetic metamaterials, often referred to as Metamaterials (MTM), have been attracting much interest over the last few years, due to their extraordinary electromagnetic properties which were previously only possible theoretically. In order to obtain such properties, MTM have to be built from artificial structures composed by objects whose size and spacing are much smaller than the incident wavelength λ , resulting in an inhomogeneous medium.

Theoretically, an inhomogeneous medium can be replaced by a homogeneous material in order to understand better the material. This homogeneous media can be characterized by two macroscopic electromagnetic parameters: electric permittivity ε and magnetic permeability μ , also referred to as constitutive parameters. This homogenization of materials is a big challenge and there are a lot of researches about extracting these parameters.

The technique used in this work is based on (NICOLSON; ROSS, 1970), which proposes to extract the electromagnetic properties of materials from the scattering parameters (S_{11}, S_{21}). However, to extract the index of refraction of metamaterials is trickier because there are infinite solutions. For that, Barroso in (BARROSO; PAULA, 2010) and (BARROSO; HASAR, 2012) discusses a method to improve the results, which is going to be used on this work.

Motivated by studies such as (PENDRY; SCHURIG; SMITH, 2006), (ERGIN *et al.*, 2010), (SILVEIRINHA; ENGHETA, 2007), this work aims to design a metamaterial with negative index of refraction while implementing methods to retrieve ε and μ in both free space and in a rectangular waveguide from the S-Parameters (S_{11}, S_{21}).

1.2 Organization of thesis

Chapter II discusses the characteristics and theoretical fundamentals of metamaterials, as well as their electric and magnetic response. Possible applications of metamaterials in waveguides and free space are also covered.

Chapter III presents the extraction of parameters of the metamaterials in both free space and rectangular waveguide. These retrieval methods are then used for later experiments.

Chapter IV focuses on design the metamaterials' cells that are used throughout the simulations and experiments. The geometries of the cells have already been studied (SMITH *et al.*, 2005; ZHANG *et al.*, 2008), but the dimensions were modified to shift the resonance frequency of the structure.

Chapter V describes the steps used to fabricate the designed cells with the PCB technique.

Chapter VI introduces the results obtained from the S-Parameters of the metamaterials' cells. The theoretical and the experimental results are then compared and analyzed.

The conclusion is presented in Chapter VII and contains suggestions for future projects.

CHAPTER

2

METAMATERIALS

Metamaterial is a term used to describe a class of artificially constructed composite materials that are able to obtain electromagnetic properties not seen in natural materials. A material composed of periodic and macroscopic structures, where desired electromagnetic response is achievable, can also be referred to as a metamaterial (SMITH *et al.*, 2001).

2.1 Effective media

All classical electromagnetic phenomena can be described by the following set of equations (GRIFFITHS; COLLEGE, 1999), also known as Maxwell's equations:

$$\begin{aligned} \nabla \times \vec{H} &= \vec{J} + \frac{\partial \vec{D}}{\partial t}, \\ \nabla \times \vec{E} &= -\frac{\partial \vec{B}}{\partial t}, \\ \nabla \cdot \vec{B} &= 0, \\ \nabla \cdot \vec{D} &= \rho, \end{aligned} \tag{2.1}$$

where $\vec{E}$ and $\vec{H}$ are, respectively, the electric and magnetic field strength while $\vec{D}$ and $\vec{B}$ are the electric and magnetic flux densities. The quantity ρ is the volume charge density and $\vec{J}$ the electric current density of any external charges.

In general, for a simple homogeneous isotropic medium (ORFANIDIS, 2002), the electric and magnetic flux densities are related to the field strengths via the *constitutive relations* (ε and μ) as

$$\vec{D} = \varepsilon \vec{E} = \varepsilon_r \varepsilon_0 \vec{E} \tag{2.2}$$

$$\vec{B} = \mu\vec{H} = \mu_r\mu_0\vec{H} \tag{2.3}$$

where $\varepsilon_0 = 8.85 \times 10^{-12}$F/m is the permittivity of vacuum and $\mu_0 = 4\pi \times 10^{-7}$H/m is the permeability of vacuum , while ε_r and μ_r refers, to the relative permittivity and permeability.

However, keeping in mind that the material is not a homogeneous medium, but actually a collection of scattering objects, it would be more convenient if this medium were replaced by an equivalent homogeneous medium. This medium should have effective parameters corresponding to the average of the local electromagnetic distributions and fields (SMITH *et al.*, 2005). This can be done when the wavelength is much larger than the scale of spatial variations in the material.

Since metamaterials consists of an array of structures whose dimensions are considerably smaller than the wavelength ($< \lambda/10$), the metamaterial will be described in this work by the effective medium parameters of permittivity ε_{eff} and permeability μ_{eff} (SMITH *et al.*, 2000).

2.2 Properties

The possibility of having both permittivity and permeability simultaneously negative is interesting because of its potential applications, which will be discussed later on this chapter. This section discusses what is necessary to achieve such properties.

2.2.1 *Negative Permeability* $\mu < 0$

In order to achieve negative permeability, the Split Ring Resonator (SRR), a conducting structure used to achieve this magnetic response (PENDRY *et al.*, 1999), can be used. The structure design is illustrated in Figure 1.

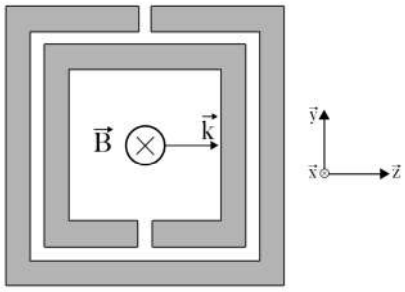

Figure 1 – Split ring resonator used to obtain negative values of permeability

Source: Based on (PADILLA; BASOV; SMITH, 2006)

In this simple representation, an SRR cell can be seen as a LC resonator. According to Faraday's Law, second equation in (2.1), the time varying magnetic field, perpendicular to the cell's plane, induces a circulating current on the conductor rings, while building charge across the ring's gap, therefore storing energy as a capacitor.

Additionally, as a normal LC resonator, the SRR has a defined resonance frequency. As the frequency of an incident wave reaches and passes this resonance, the induced current cannot follow the changes on the magnetic field and begins to lag, resulting in the desired negative response (PADILLA; BASOV; SMITH, 2006).

2.2.2 Negative Permittivity $\varepsilon < 0$

Any metal below its plasma frequency naturally acquires negative values of permittivity due to the free electrons in the metal that interact with an external electromagnetic radiation (PADILLA; BASOV; SMITH, 2006). However, it is also possible to obtain negative electric response from a distributed array of conductors, as discussed in (PENDRY *et al.*, 1999). One example of such array can be observed in Figure 2, where the electric field must be parallel with the length of the wires.

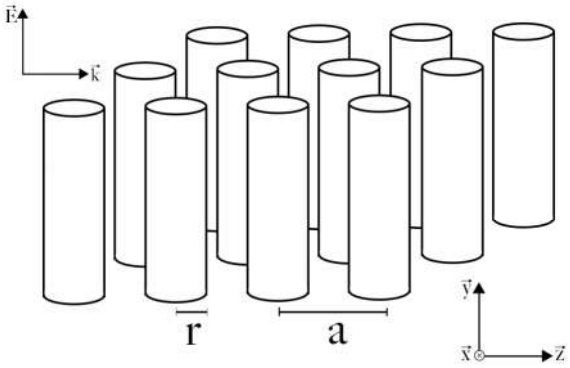

Figure 2 – Array of conductors used to obtain negative values of permittivity

Source: Based on (PENDRY *et al.*, 1999)

By changing the lattice periodicity, shape or even the conductor's radius (SMITH *et al.*, 1999), these elements can modify the electric response of the material as desired.

More details about the physical explanation of the response in an array of conductors can be seen in (PENDRY *et al.*, 1996).

2.2.3 Negative index of refraction

The complex refractive index of a media can be described by its relative parameters as

$$n = \sqrt{\mu_r \varepsilon_r} = \Re e(n) + \Im m(n) \tag{2.4}$$

where it is useful to consider the relative permittivity and permeability in terms of a complex phase,

$$\varepsilon_r = |\varepsilon_r| e^{j\theta} \tag{2.5}$$

$$\mu_r = |\mu_r| e^{j\phi} \tag{2.6}$$

However, when taking a square root function of a complex number, it is necessary to consider both a positive and negative value of the results, but only one of them corresponds to the physical response. With this logic, Eq. (2.4) becomes

$$n = \pm\sqrt{|\varepsilon_r||\mu_r|}e^{0.5(\theta+\phi)} \tag{2.7}$$

where the result chosen must be the one where the imaginary part of n is positive, in order to satisfy the conservation of energy.

Thus, when the real part of the index of refraction is negative, all the electromagnetic phenomena is affected by it (ORFANIDIS, 2002). In this media, *e.g.*, the phase velocity, Doppler shift and Snell's law (see Figure 3) are reversed. Another interesting fact is the propagation vector $\vec{k}$ is antiparallel to the Poynting vector $\vec{S}$, causing the impression that the wave is propagating in the opposite direction (ZIOLKOWSKI; KIPPLE, 2003).

Figure 3 – Reversed Snell's Law

Source: Based on https://muse.union.edu/design/acoustic-metamaterials/

Therefore, in order to achieve a negative index of refraction, the metamaterial structure used in this work inside the a waveguide consists of two sides: a split ring resonator on one side to produce negative permittivity, and an array of conductors on the other side to produce negative permeability, as shown in Figure 4.

Another type of cell also used to achieve negative refractive index is the omega-type, as displayed in Figure 15. This cell will be used on the free air experiments and is able to achieve such properties because it combines a wire and a current loop in a single structure.

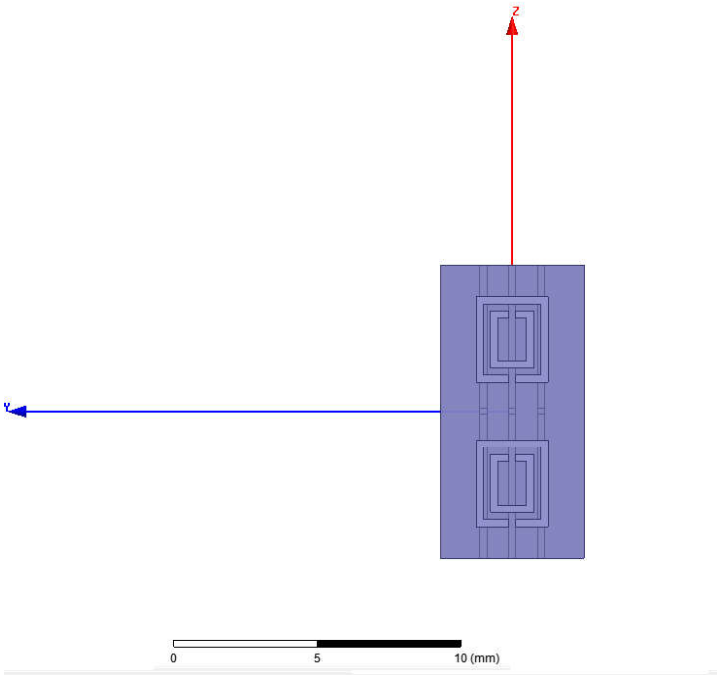

Figure 4 – Negative refractive index metamaterial used in the simulations

2.3 Classification

Having defined permittivity and permeability, it is useful now to group metamaterials into categories according to their electromagnetic properties:

- A medium with positive permittivity and permeability ($\varepsilon > 0$, $\mu > 0$) is the most common arrangement found in nature. It is also called a Right-Hand Material (RHM) because the vectors $\vec{E}$, $\vec{H}$ and propagation vector $\vec{k}$ follow the "right hand rule".
- A medium with negative permittivity and positive permeability ($\varepsilon < 0$,$\mu > 0$) is normally found in some metals below the plasma frequency or in wire structures, for example.
- A medium with negative permittivity and permeability($\varepsilon < 0$,$\mu < 0$) is also called a Left-Hand Material (LHM) because $\vec{E}$, $\vec{H}$ and propagation vector $\vec{k}$ will follow the "left hand rule", which causes the Poyinting Vector to have the opposite direction as the wave vector (PENDRY, 2000).
- A medium with positive permittivity and negative permeability ($\varepsilon > 0$, $\mu < 0$) is also known as mu negative (MNG), and is normally obtained with split ring resonators.

2.4 Applications

Metamaterials have been gaining attention because of its scientific and industrial applications. Therefore, it is relevant to briefly discuss some of the possible applications.

2.4.1 Metamaterial antennas

This class of antennas is already commercially available (DAS, 2009) and uses a LHM to reduce the electromagnetic absorption and increase the power radiated (ZIOLKOWSKI; KIPPLE, 2003). These antennas can operate in most frequency bands for mobile applications, such as Bluetooth, wireless local area network (WLAN) and upper GSM frequency bands (ALAM; FARUQUE; ISLAM, 2015).

2.4.2 MTM as sensor

Since some metamaterials exhibit strong enhancement of electromagnetic fields, it is possible to use them to improve sensor selectivity to detect small amounts of analytes (JAKŠIĆ *et al.*, 2010), e.g. when detecting

These metamaterial-based sensors are already been used in biomedical and agriculture (KITIC; RADONIC; CRNOJEVIC-BENGIN, 2012) and also as high frequency sensors (SHAMONIN *et al.*, 2006).

2.4.3 Superlenses

Governed by wave optics, conventional lenses cannot focus light onto an area smaller than a square wavelength. So, in order to focus all of the frequency components of an image, an alternative to using a conventional lens is using a LHM medium, referred to as "superlenses" (PENDRY, 2000). In this case, a single slab with the chosen thickness would bend the light to a negative angle with the surface normal, converging the rays from a source point in a second point, as displayed in Figure 5, leading to a perfect focus.

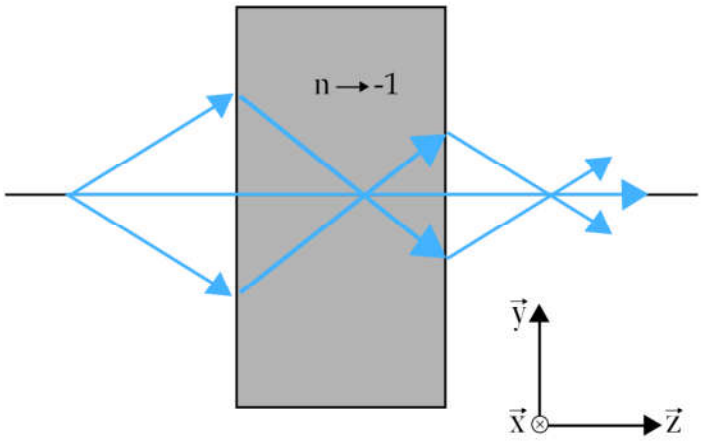

Figure 5 – LHM as superlenses

Source: Based on http://www.trnmag.com/Pendry-perfect-lens-diagram.gif

CHAPTER

3

EXTRACTION OF PARAMETERS

This chapter aims to explain the retrieval of the constitutive parameters ε and μ using the S-Parameters with the well-known Nicolson–Ross–Weir (NRW) method, which is the main focus of this work. Figure 6 shows the direction of the signals in a two-port system, where a_1 and a_2 represents the input signal while b_1 and b_2 represents the output. The Device under test (DUT) refers to the metamaterial cells being either inside the waveguide or in free space.

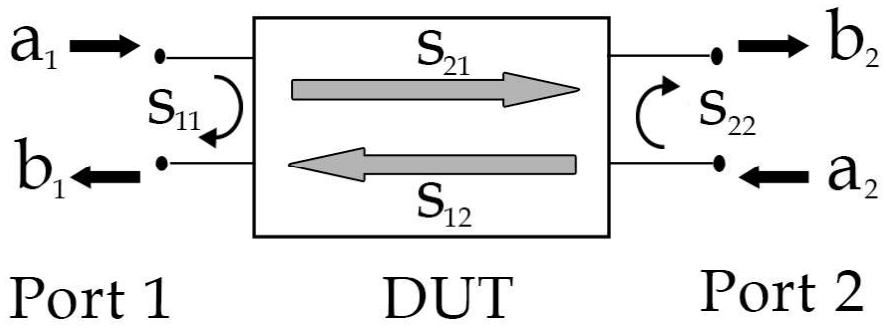

Figure 6 – Scattering Parameters

By matching Port 2, as defined in (ORFANIDIS, 2002), the coefficients can be defined as

$$S_{11} = \frac{b_1}{a_1} \tag{3.1}$$

$$S_{21} = \frac{b_2}{a_1} \tag{3.2}$$

and by matching Port 1, the parameters S_{22} and S_{12} are defined as

$$S_{22} = \frac{b_2}{a_2} \tag{3.3}$$

$$S_{12} = \frac{b_1}{a_2} \tag{3.4}$$

With the S-Parameters explained, the metamaterials interfaces are then studied in order to obtain the extraction parameters methods.

3.1 Defining the interfaces

Considering the metamaterial as a planar interface as shown in Figure 7, we can define the transmission coefficient from air (left interface) to the metamaterial (right interface) as $\tau = \tau_1$ and the reflection as $\rho = \rho_1$. For the wave coming from the metamaterial to the air interface, the transmission coefficient is $\tau^{'} = \tau_2$ and the reflection $\rho^{'} = \rho_2$.

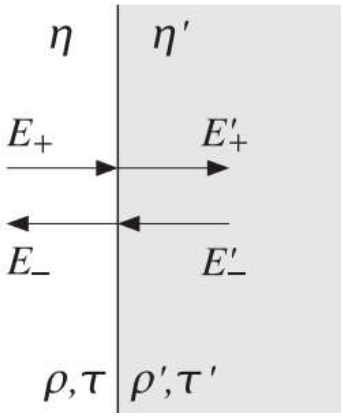

Figure 7 – Field across an interface

By definition, it is possible to relate these coefficients knowing that

$$\tau_1 = 1 + \rho_1 \text{ and } \tau_2 = 1 + \rho_2 \tag{3.5}$$

and since the interfaces are the same, the coefficients of reflection are defined as

$$\rho_1 = \frac{\eta - \eta^{'}}{\eta + \eta^{'}} \quad , \quad \rho_2 = \frac{\eta^{'} - \eta}{\eta^{'} + \eta} \rightarrow \boxed{\rho_1 = -\rho_2} \tag{3.6}$$

By substituting Equation 3.5 into Equation 3.6 a useful relation is obtained:

$$\boxed{\tau_1 \tau_2 = 1 - \rho_1^2} \tag{3.7}$$

3.2 Defining the S-Parameters

One way to define the S-Parameters is by analyzing the multiple reflections within a material, to see how much of an incident wave is reflected or transmitted through. These multiple reflections are represented in Figure 8, where the single slab is the metamaterial with unknown ε_r and μ_r.

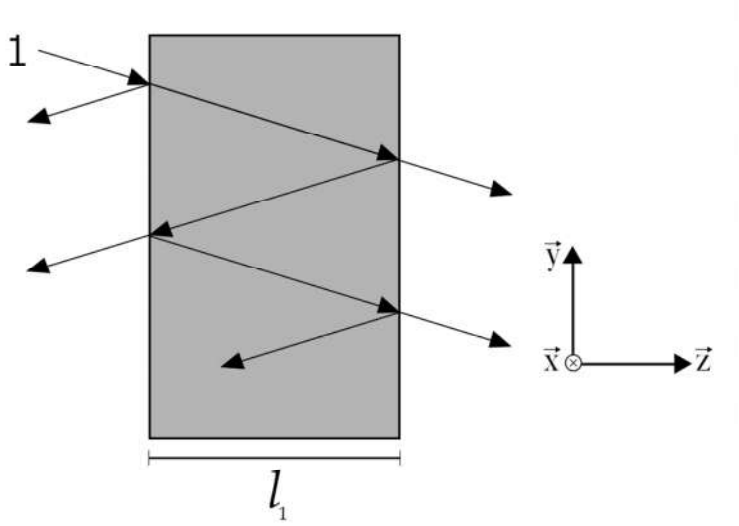

Figure 8 – Multiple reflections within a slab

Source: Based on (ORFANIDIS, 2002)

From Figure 8, an incident wave on the top left corner reaches the left interface and gets transmitted, picking up a coefficient τ_1 and is then transmitted on the second interface, changing its amplitude to $\tau_1\tau_2 e^{-j\delta}$, where $\delta = kl_1$ and k is the propagation vector, so that $e^{-j\delta}$ refers to a phase shift after the wave goes across the slab with a thickness of l_1 (ORFANIDIS, 2002). But due to the multiple reflections inside the slab, this wave is not the only one transmitted through. At the second interface, the wave with an amplitude of $\tau_1 e^{-j\delta}$ also gets reflected twice in the metamaterial-air interface and only then the transmission will happen. This way, the second transmitted wave has the amplitude of $\tau_1\rho_2\rho_2\tau_2 e^{-j3\delta}$.

Thus, the scattering parameter S_{21}, which is how much power is transmitted through the material, is

$$S_{21} = \tau_1\tau_2 e^{-j\delta} + \tau_1\rho_2^2\tau_2 e^{-j3\delta} + \tau_1\rho_2^4\tau_1 e^{-j5\delta} + \ldots \tag{3.8}$$

and since it is an infinite sum, it is possible to write equation 3.8 as:

$$S_{21} = \sum_{i=0}^{\infty} \tau_1\tau_2\rho_2^{2i} e^{-j\delta(1+2i)} = \tau_1\tau_2 e^{-j\delta} \sum_{i=0}^{\infty} (\rho_2^2 e^{-j2\delta})^i \tag{3.9}$$

For a good approximation, it is known that $\rho_2^2 e^{-j2\delta} < 1$, so it is possible to use the series

$$\sum_{k=0}^{\infty} r^k = \frac{1}{1-r} \text{ for } r < 1 \tag{3.10}$$

so that the S_{21} term becomes

$$S_{21y} = \frac{\tau_1 \tau_2 e^{-j\delta}}{1 - \rho_2^2 e^{-j2\delta}} \tag{3.11}$$

By last, using 3.6 and 3.7 in Equation 3.11, it is obtained

$$\boxed{S_{21} = \frac{e^{-j\delta}\left(1 - \rho_1^2\right)}{1 - \rho_1^2 e^{-2j\delta}}} \tag{3.12}$$

Now that the parameter S_{21} is known, it is necessary to calculate how much of the wave is reflected off the slab, which is the S_{11} parameter.

The first wave that gets reflected has amplitude ρ_1 and part is transmitted with amplitude τ_1. The transmitted wave then reaches the other interface, is reflected, comes back and gets transmitted, now with an amplitude $\tau_1 \rho_2 \tau_2 e^{j2\delta}$. Following this, we can write the scattering parameter S_{11} as

$$S_{11} = \rho_1 + \tau_1 \rho_2 \tau_2 e^{-j2\delta} + \tau_1 \rho_2^3 \tau_2 e^{-j4\delta} + \ldots \tag{3.13}$$

$$S_{11} = \rho_1 + \sum_{i=0}^{\infty} \tau_1 \tau_2 \rho_2^{2i+1} e^{-j2\delta i} = \rho_1 + \tau_1 \tau_2 \rho_2 \sum_{i=0}^{\infty} (\rho_2^2 e^{-j2\delta})^i \tag{3.14}$$

Since (3.14) contains the term $\rho_2^2 e^{2i\delta} < 1$, it is possible to reuse the same approximation from (3.10), so S_{11} becomes

$$S_{11} = \rho_1 + \frac{\tau_1 \tau_2 \rho_2}{1 - (\rho_2^2 e^{-j2\delta})} \tag{3.15}$$

Again, using (3.6) and (3.7) and arranging the variables, we have

$$\boxed{S_{11} = \frac{\rho_1 \left(1 - e^{-2j\delta}\right)}{1 - \rho_1^2 e^{-2j\delta}}} \tag{3.16}$$

3.3 Extraction inside a waveguide

3.3.1 Defining the parameters

Figure 9 shows a waveguide section containing the metamaterial with unknown permittivity and permeability and width d_{cell}. Assuming that there is only one propagating mode inside

the waveguide in the $\vec{z}$ direction, which is the dominant $TE_{mn} = TE_{10}$, the following fields are obtained (BALANIS, 2012):

$$E_y = -\frac{\beta_x}{\varepsilon}\sin(\beta_x x)\cos(\beta_y y)e^{-j\beta_z z} \tag{3.17}$$

$$H_x = \frac{\beta_x \beta_z}{\omega\mu\varepsilon}\sin(\beta_x x)\cos(\beta_y y)e^{-j\beta_z z} \tag{3.18}$$

$$H_z = -j\frac{\beta_c}{\omega\mu\varepsilon}\cos(\beta_x x)\cos(\beta_y y)e^{-j\beta_z z} \tag{3.19}$$

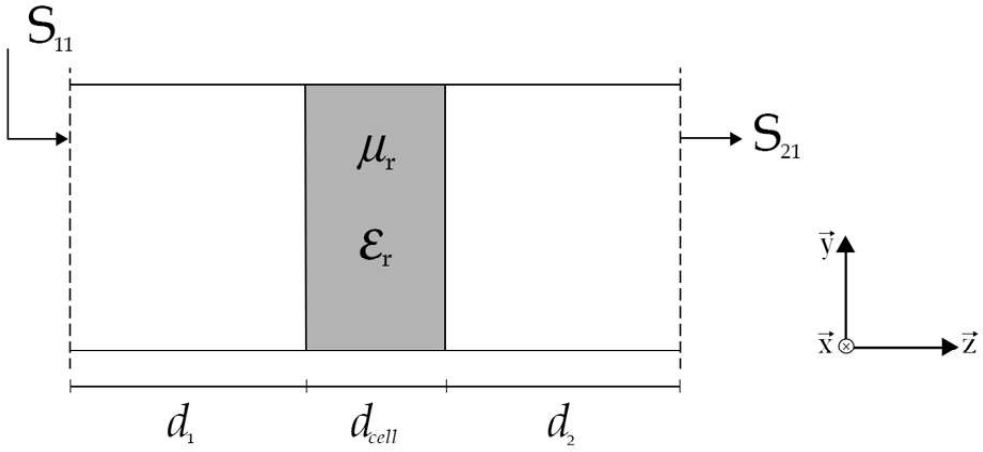

Figure 9 – Representation of the waveguide parameter extraction problem

where $\beta_x, \beta_y, \beta_z$ are the respective propagation vectors in each direction, E_y is the electric field in the $\vec{y}$ direction, $H_x and H_z$ are the magnetic field in the $\vec{x}$ and $\vec{z}$ directions.

Since the excited mode is TE_{10}, the propagation vectors are written as

$$\beta_x = \frac{m\pi}{a} = \frac{\pi}{a} \tag{3.20}$$

$$\beta_y = \frac{n\pi}{b} = 0 \tag{3.21}$$

$$\beta_z = \sqrt{\omega^2\mu\varepsilon - \beta_x^2 - \beta_y^2} = \sqrt{\omega^2\mu\varepsilon - (\frac{\pi}{a})^2} \tag{3.22}$$

where the cutoff propagation vector β_c is

$$\beta_c = \sqrt{\beta_x^2 + \beta_y^2} = \frac{\pi}{a} \tag{3.23}$$

With the fields of (3.17 - 3.19) propagating through the metamaterial and the air, the boundary conditions are applied. By using the NRW method (HASAR *et al.*, 2014), it is possible to retrieve the parameters ε_r and μ_r from the material inside the waveguide with the help of (3.12) and (3.16), defining

$$\rho_1 = \rho = \frac{Z - Z_0}{Z + Z_0} \quad \text{and} \quad e^{-jkd_{cell}} = \tau_1 = e^{-\gamma d_{cell}} \tag{3.24}$$

where Z represents the impedance of the metamaterial and Z_0 the impedance of the empty waveguide, defined respectively as

$$Z = \frac{j\omega\mu_0\mu_r}{\gamma} \quad , \quad Z_0 = \frac{j\omega\mu_0}{\gamma_0} \tag{3.25}$$

and γ and γ_0 represent the propagation factors

$$\gamma = j\sqrt{\frac{\omega^2\varepsilon_r\mu_r}{c^2} - \beta_c^2} \quad , \quad \gamma_0 = j\sqrt{\frac{\omega^2}{c^2} - \beta_c^2} \tag{3.26}$$

where c is the speed of light.

3.3.2 Analyzing the problem

As explained in (NICOLSON; ROSS, 1970), it is possible to obtain the reflection coefficients from the scattering parameters from

$$R(f) = X(f) \pm \sqrt{X(f)^2 - 1} \tag{3.27}$$

where

$$X(f) = \frac{S_{11}(f)^2 - S_{21}(f)^2 + 1}{2S_{11}(f)} \tag{3.28}$$

The reflection coefficient must be $|R(f)| \leq 1$, so the $\pm$ sign in 3.27 must be chosen accordingly. The transmission coefficient can be written as

$$T_1(f) = \frac{S_{11}(f) + S_{21}(f) - R(f)}{1 - R(f)(S_{11}(f) + S_{21}(f))} \tag{3.29}$$

However, (3.29) can lead to some ambiguities when retrieving the parameters $\varepsilon_r(f)$ and $\mu_r(f)$ (BARROSO; PAULA, 2010). To solve this, the following equation is used:

$$T(f) = \frac{1}{2\pi d_{cell}}\left(jln(|T_1(f)|) - \phi - 2n\pi\right) \tag{3.30}$$

where ϕ is the phase of $T_1(f)$, d_{cell} is the sample width and n is an integer number representing the branch index.

Knowing that $Z(f)/Z_0 = (1+R(f))/(1-R(f))$ and combining equations (3.25) and (3.26), it is possible to recast the complex permeability $\mu_r(f)$ of the media inside a waveguide as

$$\boxed{\mu_r(f) = \lambda_{0g} T(f) \left(\frac{1+R(f)}{1-R(f)} \right)} \tag{3.31}$$

where

$$\lambda_{0g} = \frac{\lambda_0}{\sqrt{1-(\lambda_0/\lambda_c)^2}} \tag{3.32}$$

Now, with (3.31) and (3.32), it is possible to obtain the permittivity $\varepsilon_r(f)$ as

$$\boxed{\varepsilon_r(f) = \frac{\lambda_0 \left(T(f)^2 + \lambda_c^{-2} \right)}{\mu_r(f)}} \tag{3.33}$$

The index of refraction of this media can easily be obtained by multiplying both constitutive relations as

$$\boxed{n(f) = \sqrt{\varepsilon_r(f)\mu_r(f)}} \tag{3.34}$$

One correction is necessary when analyzing the refractive index which is that the imaginary part cannot be negative. So if this happens, $n(f) = -n(f)$ must be applied.

The normalized impedance of the media can be written as follows:

$$\boxed{Z(f) = \frac{1+R(f)}{1-R(f)}} \tag{3.35}$$

It is worth remembering from (3.35) is that the real part of $Z(f)$ cannot be smaller than zero. In this case, $Z(f) = -Z(f)$ should be applied.

3.3.3 Phase correction

Since there is a distance between the input port of the waveguide and the metamaterial surface, these distances must be included. The waveguide used is symmetrical, so $d_1 = d_2$, and the waveguide length is $d_{wg} = d_1 + d_{cell} + d_2$, where d_{cell} is the cell width and its center is d_{off} away from the center of the waveguide. In the simulation it is possible to achieve $d_{off} = 0$, but in the experiments the cell might not be perfectly centered, so it's necessary to measure d_{off}.

For this reason, the corrected S-Parameters S'_{11} and S'_{21} become

$$S_{11}(f)' = S_{11}(f)e^{-j\beta_z\left(d_{wg}-d_{cell}-2d_{off}\right)} \tag{3.36}$$

$$S_{21}(f)' = S_{21}(f)e^{-j\beta_z\left(d_{wg}-d_{cell}\right)} \tag{3.37}$$

3.3.4 Matlab implementation

In order to extract permittivity, permeability, impedance and index of refraction during this work, a Matlab function was implemented, which can be found in Appendix A. The necessary inputs are cell width, branch index number, the vectors S_{11}, S_{21} and frequency.

3.4 Extraction in free space

3.4.1 Defining the parameters

Following the equations for the extraction inside a waveguide, measurements on materials in free space environment are similar. Figure 10 shows an example of material with unknown constitutive parameters surrounded by air and how the S-Parameters can be obtained.

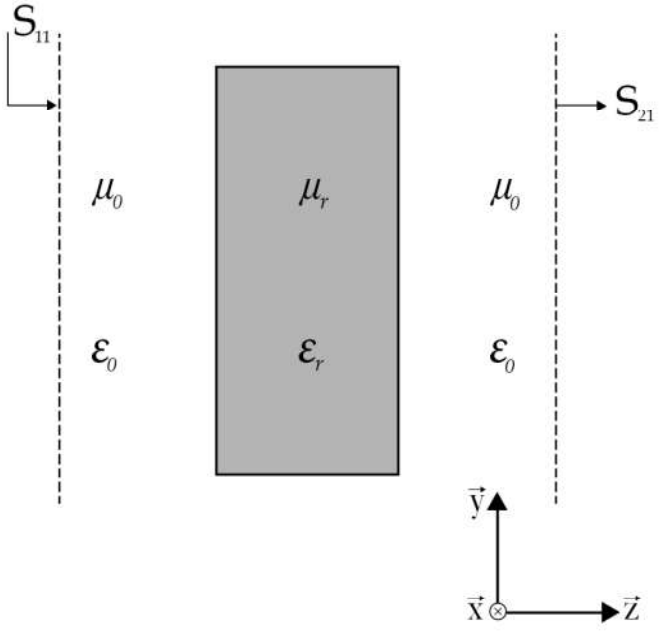

Figure 10 – Representation of the extraction in free space

With reference to (3.16) and (3.12), it is possible to write the S-Parameters for this problem as

$$S_{21} = \frac{\tau(1-\rho^2)}{1-\rho^2\tau^2} \quad , \quad S_{11} = \frac{\rho(1-\tau^2)}{1-\rho^2\tau^2} \tag{3.38}$$

where the coefficients ρ and τ can be written, again, as

$$\rho = \frac{Z-Z_0}{Z+Z_0} \quad , \quad \tau = e^{-\gamma\delta} \tag{3.39}$$

3.4.2 Analyzing the problem

Since in free space there is no cutoff frequency, $f_c = 0$ or $\lambda_c \to \infty$, so (3.32) is rewritten as

$$\lambda_{0g} = \lambda_0 \tag{3.40}$$

resulting in the permittivity

$$\boxed{\varepsilon_r(f) = \frac{\lambda_0 T(f)^2}{\mu_r(f)}} \tag{3.41}$$

and the permeability

$$\boxed{\mu_r(f) = \lambda_0 T(f)\left(\frac{1+R(f)}{1-R(f)}\right)} \tag{3.42}$$

Comparing with the extraction inside the waveguide, the reflection coefficient in free space remains the same, while the transmission requires some adjustments (BARROSO; HASAR, 2012) as follows

$$R(f) = X(f) \pm \sqrt{X(f)^2 - 1} \quad , \quad X(f) = \frac{S_{11}(f)^2 - S_{21}(f)^2 + 1}{2S_{11}(f)} \tag{3.43}$$

$$T_1(f) = \frac{S_{21}(f)}{1 - S_{11}(f)R(f)} \quad , \quad T(f) = \frac{1}{2\pi d_{cell}}\left(jln(|T(f)|) - \phi - 2n\pi\right) \tag{3.44}$$

where ϕ is the phase of $T_1(f)$ and d_{cell} is the sample width and n is the integer denoting the branch index.

3.4.3 Matlab implementation

The Matlab code for the extraction in free space can be found in Appendix B.

CHAPTER

4

DESIGN AND SIMULATION

A simulation-based retrieval method is very appealing when designing metamaterials because even though the structures are complex, the physical parameters of the dielectric substrate and conductors are known. Thus, the effective parameter of the material can be calculated more efficiently than building the structures for measuring and analyzing, as discussed in Chapter 5.

The simulations are carried out in the software Ansys High Frequency Structural Simulator (HFSS), available at the Laboratory of Telecommunications at USP São Carlos. This software is based on the the finite element method, which is a very useful numerical simulation technique to solve electromagnetic problems.

4.1 Inside the waveguide

The geometry of the cells used inside the waveguide is based on (BARROSO; HASAR, 2012). This structure consists of two types of conducting elements: a split-ring resonator and an array of three wires, as shown in Figure 11.

Using HFSS to build the metamaterial, the dielectric board chosen is a 0.85 mm-thick Rogers RT/duroid 5870 ($\mu_r = 1$, $\varepsilon_r = 2.33$, dielectric tangent 0.0012), which is available in HFSS 15.0 and also available for fabrication in the Laboratory, while the conductive lines are assumed as a perfect conductor sheets. The dimensions used are listed in Table 1 while the HFSS structure is shown in Figure 12.

The waveguide dimensions are based on a WR-90 waveguide, with dimensions $a =$ 22.86mm, $b = 10.17$mm, so five cells from (see Figure 12) are inserted inside the waveguide, separated by 4.5 mm. This waveguide simulated has a length of 100 mm, and its ends are defined as excitation ports, as shown in Figure 13.

In order for the waveguide to respond as expected, the side boundaries (Plan yz) and top and bottom (Plan XY) are defined as a Perfect Electric Conductor (PEC), as shown in Figures

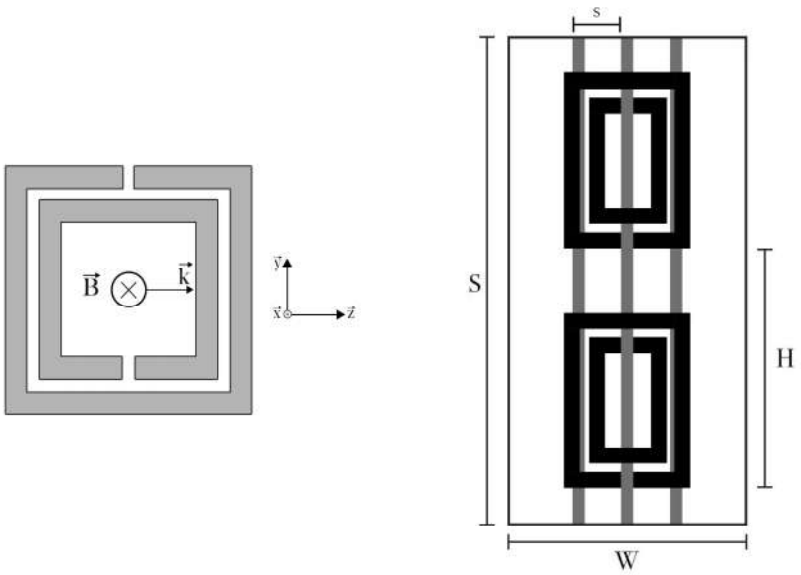

Figure 11 – Designed cell used inside the waveguide

Symbol on Figure 11	Description	Dimension
W	Width of the cell	2.45 mm
H	Height of the cell	10.17 mm
w	Width of SRR	2.45 mm
h	Height of SRR	3.75 mm
g	Gap	0.25 mm
c	Line thickness	0.25 mm
d	Separation between rings	0.25 mm
S	Separation between the SRR	5.0 mm
s	Separation between the wires	1.0 mm

Table 1 – Dimensions of the designed cell to use in the waveguide experiment

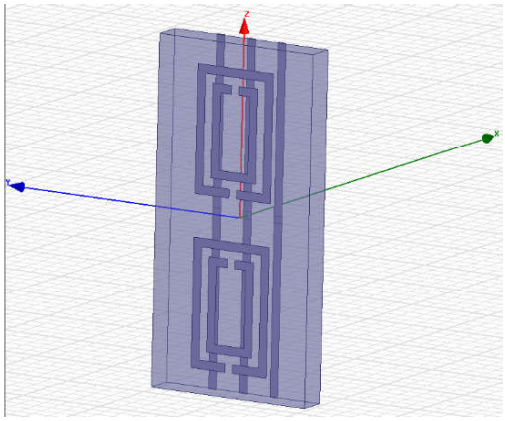

Figure 12 – One metamaterial cell drawn using HFSS

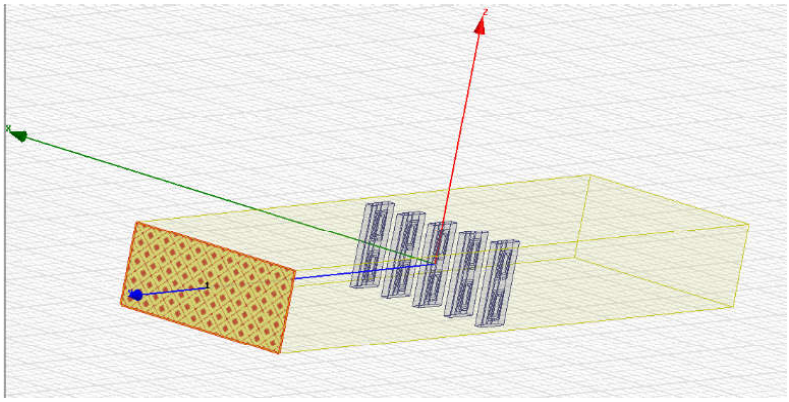

Figure 13 – Waveguide with port excitation and five metamaterials' cells

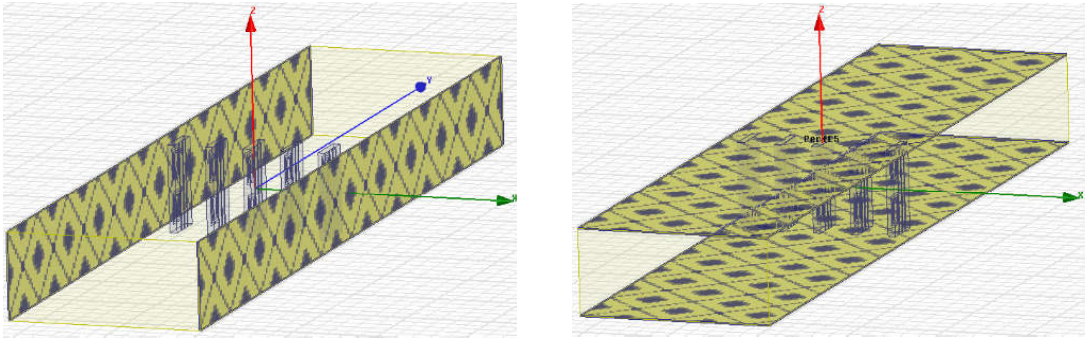

Figure 14 – Boundaries defined as PEC in the simulated waveguide. (a) Side boundaries and (b) Top and bottom boundaries

14(a) and 14(b), respectively.

4.2 Free space

For the free space experiments, the geometry used is the omega-type metal inclusion, based on (ZHANG *et al.*, 2008), as shown in Figure 15. This Figure also shows where the excitation ports are, together with the boundaries assigned as PEC and Perfect Magnetic Conductor (MC).

The dielectric board is a 0.49 mm-thick Rogers RO4003 ($\varepsilon_r = 3.55$, $\mu_r = 1$, dielectric tangent 0.0027), available in the Laboratory and also in HFSS 15.0.

With the input and output ports, PEC and PMC boundaries displayed in Figure 15, the omega-type cell was implemented in HFSS using the dimensions listed in Table 2, as seen in Figure 16.

The dimensions indicated in Figure 15 are in Table 2.

The dielectric substrate is 6 mm x 8 mm, where the smaller size is parallel to the base of the omega-cell.

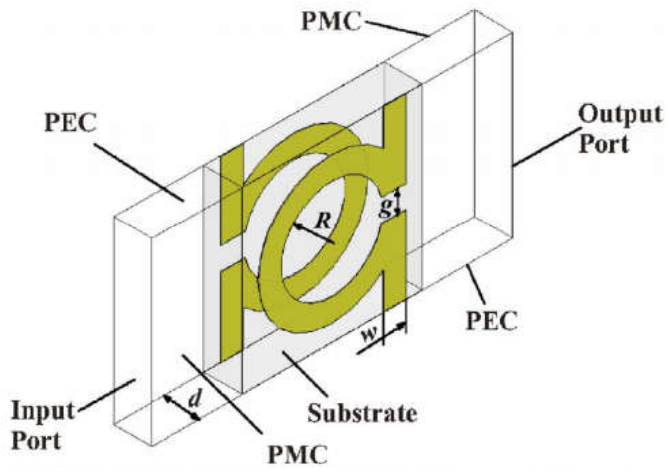

Figure 15 – Omega-type cell used for free space experiments

Symbol on Figure 15	Description	Dimension
d	Thickness	0.49 mm
g	Gap	0.3 mm
R	Radius	1.75 mm
w	Width	0.5 mm
	Width of the substrate	8.0 mm
	Height of the substrate	6.0 mm

Table 2 – Dimensions of the designed cell to use in the free space experiment

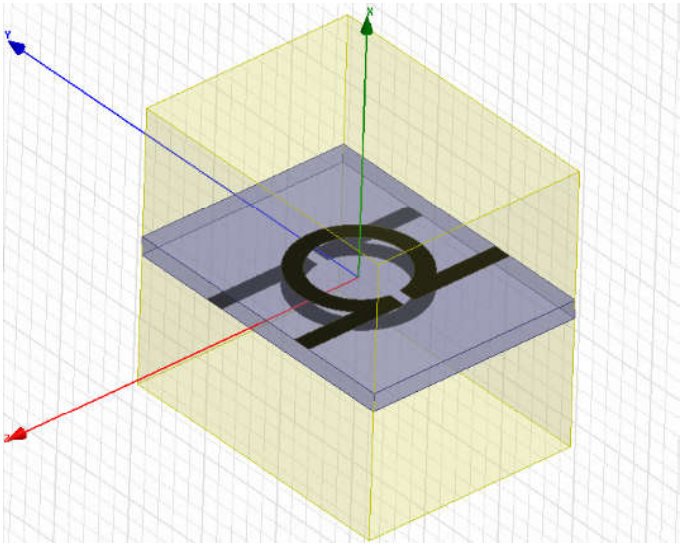

Figure 16 – Omega-type cell implemented in HFSS

CHAPTER

5

FABRICATION

This chapter describes the most common and reliable method to produce printed circuit boards: the photographic method. In spite of the necessity to dilute some of the chemicals involved, the photographic method can produce a good quality Printed Circuit Board (PCB), even for small dimensions. This chapter is divided into 5 sections, which are the steps to complete the fabrication: Layout, Preparation, UV Exposure, Development and Etching. This chapter discusses the fabrication process of the boards to be used inside the waveguide.

5.1 Layout

The PCB Layout was done using the dimensions of 1 and by inverting the colors of the HFSS design from Figure 11, so that the white part represents the conductors and the black part, the dielectric. This layout design was then prepared to be printed, as displayed on Figure 17.

To assure that the board has a good quality, it is necessary that the minimal amount of UV light propagates through the black part of the layout. For this, the chosen printer must have as many Lines per Inch (LPI) as possible to increase the resolution. This layout was printed on a Laserstar film, which is recommended for PCB design.

5.2 Preparation

With the layout ready, the board must be prepared for the UV Exposure. Since the layout is for both sides of the cell, this process must be carried out for one side at a time. After that, the other side of the board must be prepared following the same process. This section describes the preparation of the SRR side, so first it's necessary to protect the side for the array of conductors from the chemicals by applying, for example, adhesive tape.

To make the board sensitive to UV Exposure, it is first necessary to apply Liquid

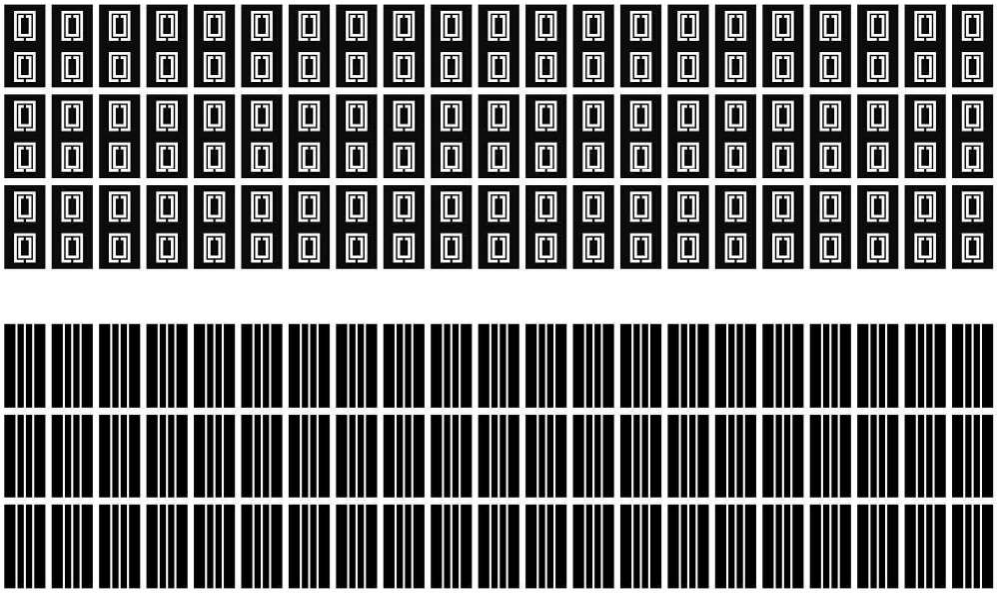

Figure 17 – PCB Layout printed for manufacturing

Photoresist, which is a light-sensitive material. The problem with this step is that the Photoresist should spread homogeneously on the board, avoiding problems with the next steps. So, to make this easier, the board is glued on to a 12V DC Motor, and kept inside a bucket to reduce photoresist spills, as shown in Figure 18.

The Liquid Photoresist is poured, while the speed of the motor is increased, as displayed in Figure 19 (a). After a few attempts, it becomes apparent that slowly increasing the speed while pouring the Liquid produces a regular spreading of liquid on the board. Figure 19 (b) shows the board with a smooth layer of Liquid Photoresist.

After that, it is necessary to wait for the liquid to dry. During the first attempts, the thermal press can be used to speed up the drying process. However, a room with no light for at least 12 hours is more efficient for this step.

5.3 UV Exposure

The printed PCB Layout from Figure 17 is then taped on to a glass panel in order to ensure that the Layout is straight on top of the board, as seen in Figure 20. Next, the board is exposed to a 25W fluorescent ultraviolet light bulb for 5 minutes, from a distance of 15 cm. Figure 21 shows the configuration for this step.

Figure 18 – PCB board and a 12V DC Motor before applying the liquid photoresist

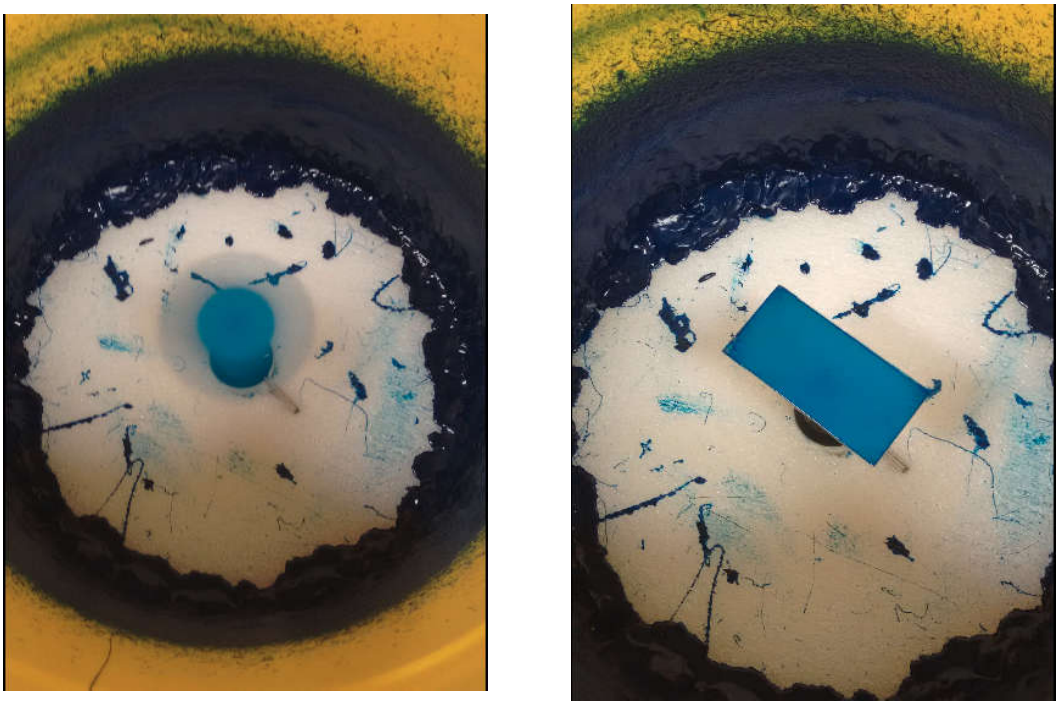

Figure 19 – Preparation of the board with Liquid Photoresist, (a) Application of Liquid Photoresist on the board, (b) PCB board ready to be exposed to the UV.

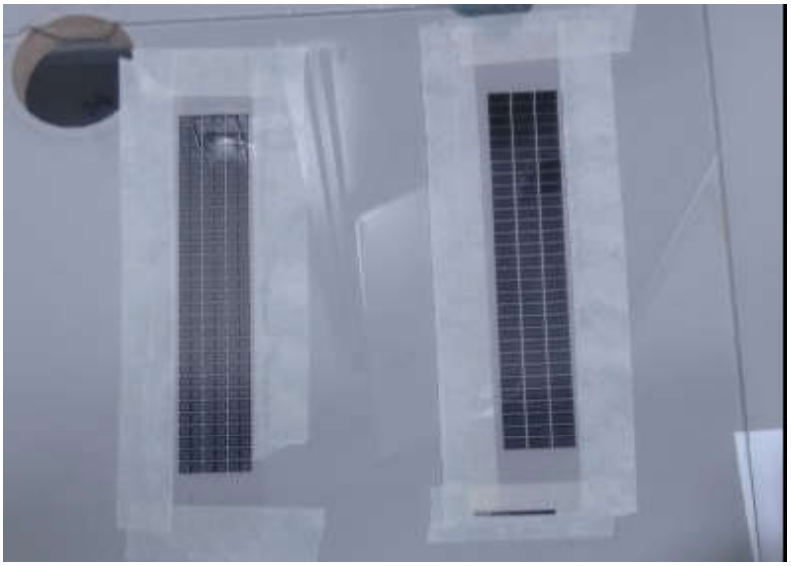

Figure 20 – Set up for the UV exposure

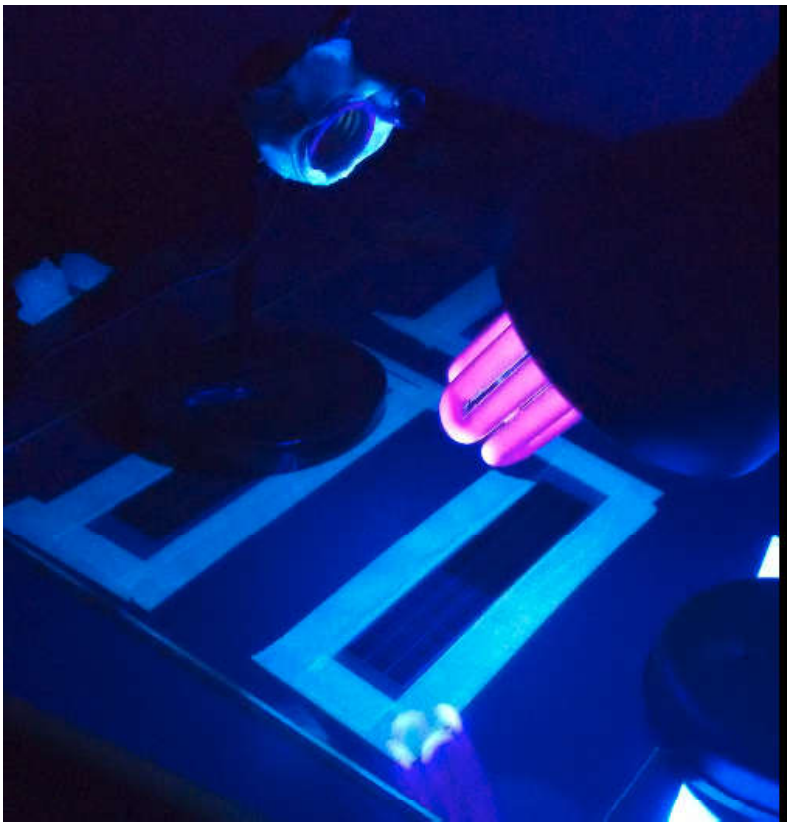

Figure 21 – UV Exposure on the board

5.4 Development

After the exposure, a solution of 1% Sodium Hydroxide is used to develop the board. This solvent can be made by adding 5 g of Sodium Hydroxide pellets to 500 mL of water and mixed with the board for 3 minutes.

Since the SRR and array of conductors got exposed to the UV Light, the Liquid Photoresist will harden these areas and remain on the board after the development. Meanwhile, since the dark areas of the layout did not receive the UV light, the photoresist on these parts will dissolve.

5.5 Etching

The developed PCB is etched in a solution of 500 grams of Iron Perchlorate dissolved in 1 litter of water for 30 minutes.

After the etching, the board is inserted into a solution with Photoresist Removal and water. This step will remove all the remaining Photoresist from the board, so it is ready for use, as shown in Figure 22.

Figure 22 – Etched board ready to use

After this, it is possible to start the preparation process again for the other side of the board, while protecting the already etched side.

CHAPTER

6

RESULTS

This Chapter first presents the results obtained through measurements and then compare them with the results obtained with the simulations of the fabricated metamaterials for both the waveguide and free-space samples.

6.1 Inside the waveguide

6.1.1 Measurements

With the metamaterial's cells from Chapter 5 designed and fabricated, the measurements are then carried out in the Laboratory of Telecommunication to obtain the Scattering Parameters using the Vector Network Analyzer ZVA 40 from *Rohde & Shwarz*. The cells are inserted in a WR-90 waveguide with attenuators connected to reduce internal reflections, as shown in Figure 23. The network analyzer was first calibrated using the TLR mode, following the instructions of the equipment, and after the scattering parameters were measured.

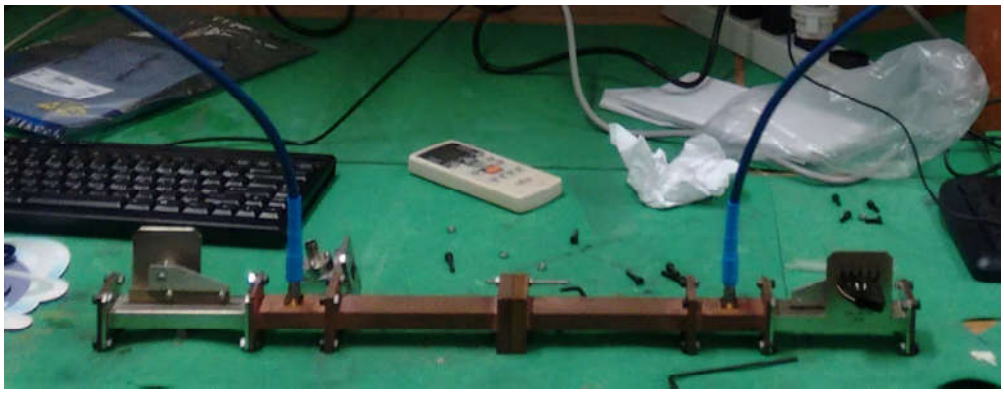

Figure 23 – Set up to measure the S-Parameters with the cells inside the waveguide

The Network Analyzer is then adjusted to measure the S-Parameters S_{11} and S_{21} over

the frequency range from 8.1 to 8.55 GHz. The data obtained can be be seen in Figure 24

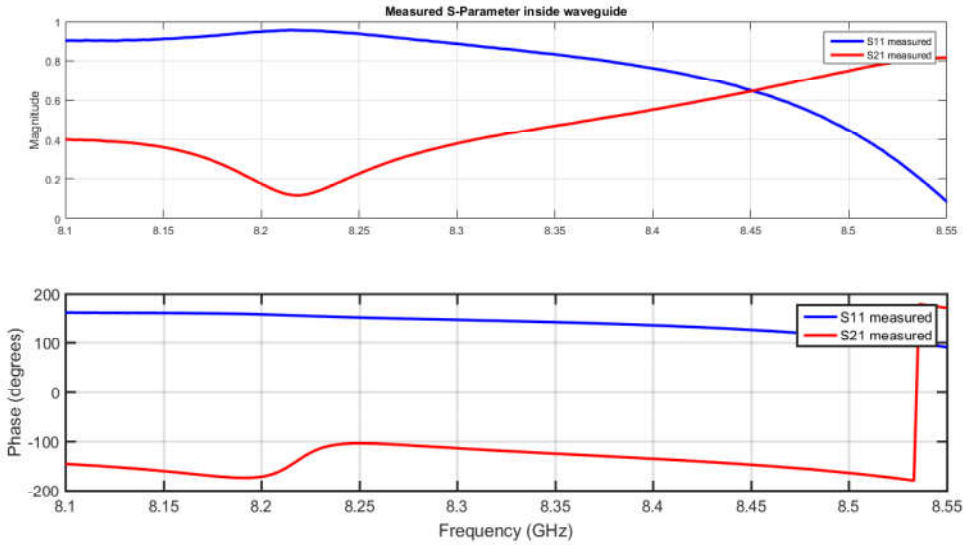

Figure 24 – Measured S-Parameters of the metamaterial cell inside the waveguide

For the simulated measurements, the resonance frequency is obtained again analyzing the variation of the phase of S_{21}, obtaining $f_c = 8.23$ GHz, which is lower than the designed resonance frequency. This shift of frequency is likely to occur due to fabrication mistakes (e.g. line thickness different or corners not straight) or measurement problems (e.g. cells separated differently).

With the measured S-Parameters, the constitutive parameters are then obtained, as shown in Figure 25 and from them the index of refraction n is retrieved and plotted in Figure 26.

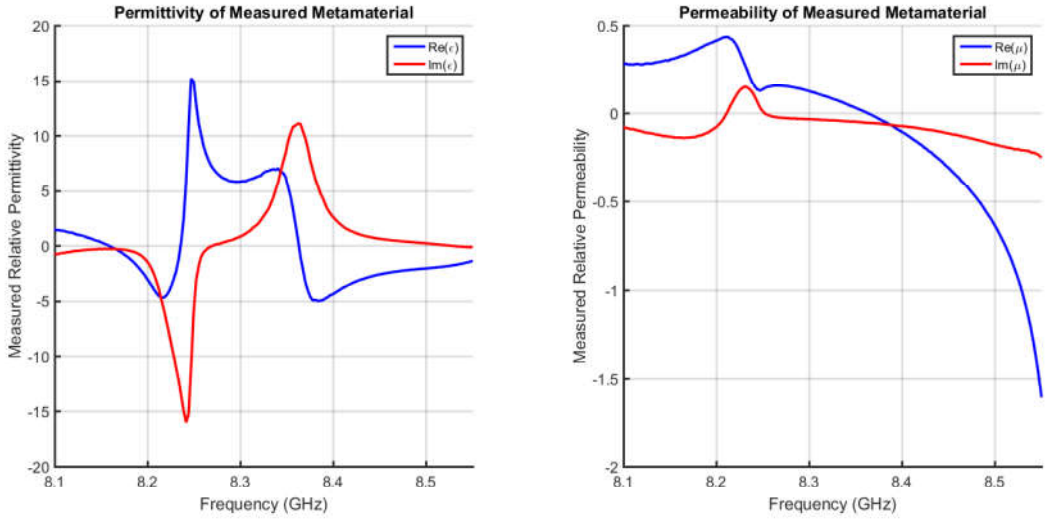

Figure 25 – Constitutive parameter obtained from measured metamaterial inside waveguide. (a) Relative permittivity, (b) Relative permeability.

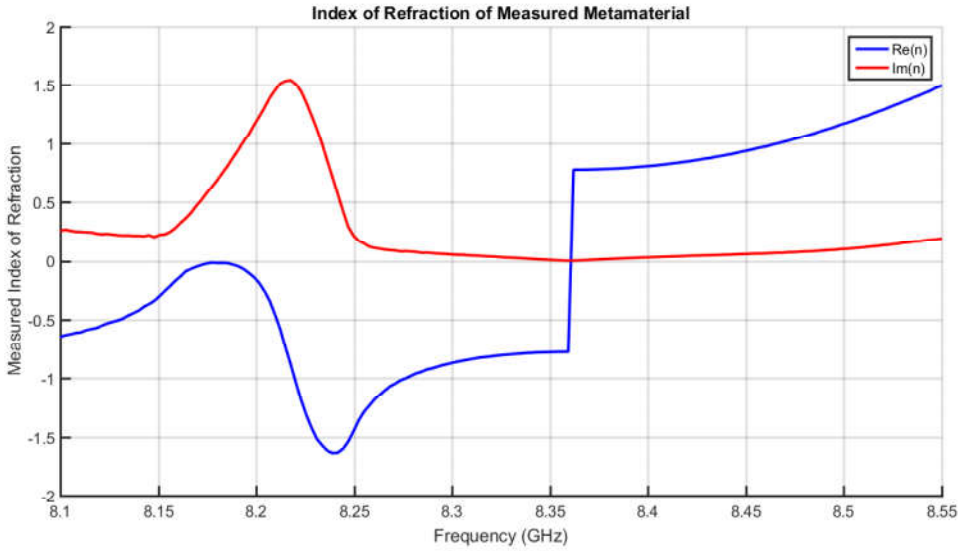

Figure 26 – Measured index of refraction of the metamaterial cell inside the waveguide

Although the constitutive parameters obtained from Figures 25 are slightly different from the simulated parameters in Figure **??**, it is still possible to identify a resonance frequency, where the refractive index is negative.

From Figure 26, it can be seen that in the frequency range from 8.18 to 8.35 GHz the real part of the index of refraction < -2, reaching a minimum at 8.4 GHz with $Re(n) = -3.38$. Also notice that the phase remains the same after the f_c.

For further analysis, the impedance is also retrieved and can be seen in Figure 27. Differently from the impedance simulated, the imaginary part of the measured impedance does not remain constant after the resonance frequency.

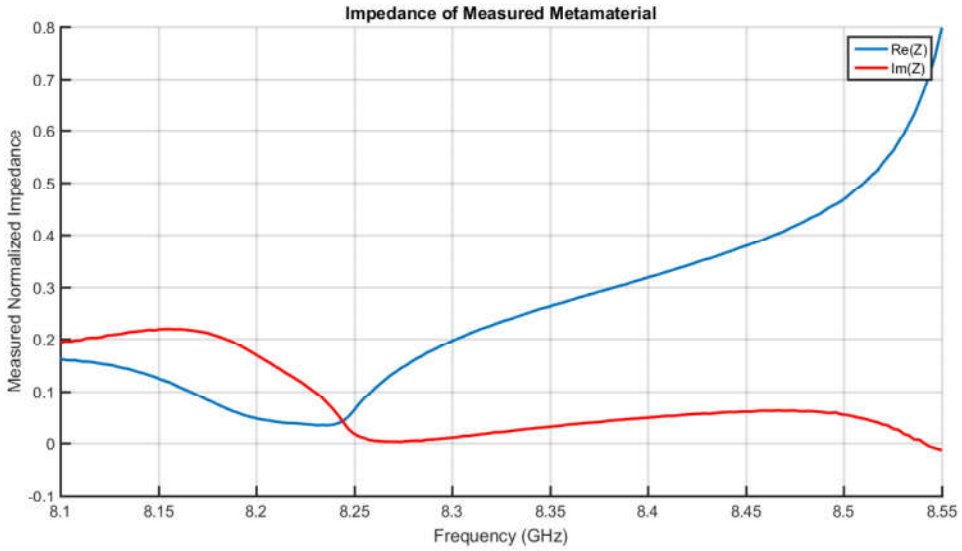

Figure 27 – Measured impedance of the metamaterial cell inside the waveguide

6.1.2 Simulated Parameters

With the simulated cells already detailed in Chapter 4, the Scattering Parameters are obtained with HFSS and exported to a *.m* file. The plot of the magnitude and phase of S_{11} and S_{21} are displayed in Figure 28.

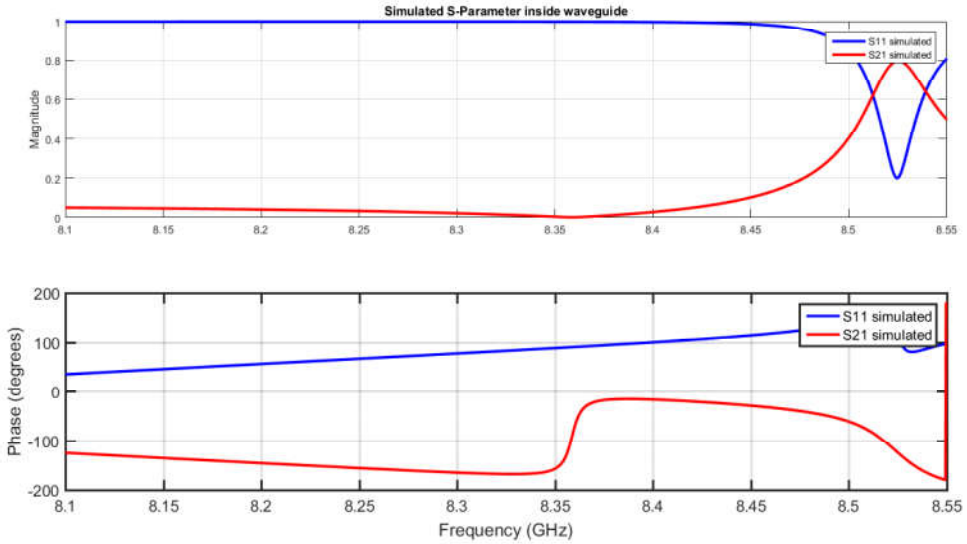

Figure 28 – Simulated S-Parameters of the metamaterial cell inside the waveguide

Figure 28 has the expected pattern for a metamaterial with negative index of refraction, as described earlier in this Chapter. However, the simulation in Section 4 was not an accurate version of the experiment, which culminated in distinct results.

At first, the simulation ports should not be matched ports, but actually they should represent the attenuators used in the experiment, which would need a deeper study of the HFSS software. The simulation was also a very complex, needing more mesh numbers for the complex structure of the waveguide with the cells inside. However, this complexity also increases the amount of computer processing and the duration of the simulations. This was a big problem when trying to obtain new results. Therefore, it was decided not to publish the simulated results obtained, since they do not represent the actual phenomena.

6.2 Free space

As detailed in Chapter 4, the free space experiment uses the Omega cell shown in Figure 29. In theory, it is possible to use a single Omega cell (Figure29b) with periodic boundary conditions to simulate an infinite arrangement of cells. But due to impracticability of an infinite arrangement, the experimental part results are obtained from a finite number of cells, as shown in Figure 29a.

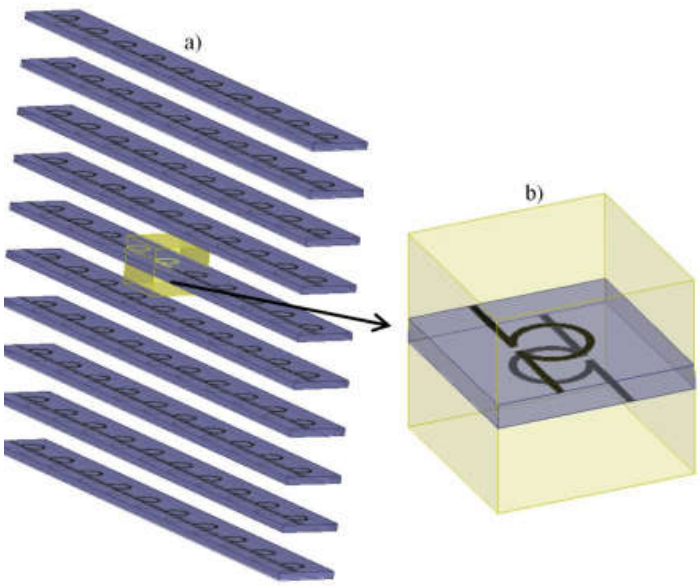

Figure 29 – 3-D representation of the metamaterial used for free-space measurements

Source: (MOTA, 2015)

6.2.1 Simulated Parameters

To obtain the S-Parameters, the HFSS simulation of Figure 16 was used and the resulting S_{11} and S_{21} plotted in Figure 30.

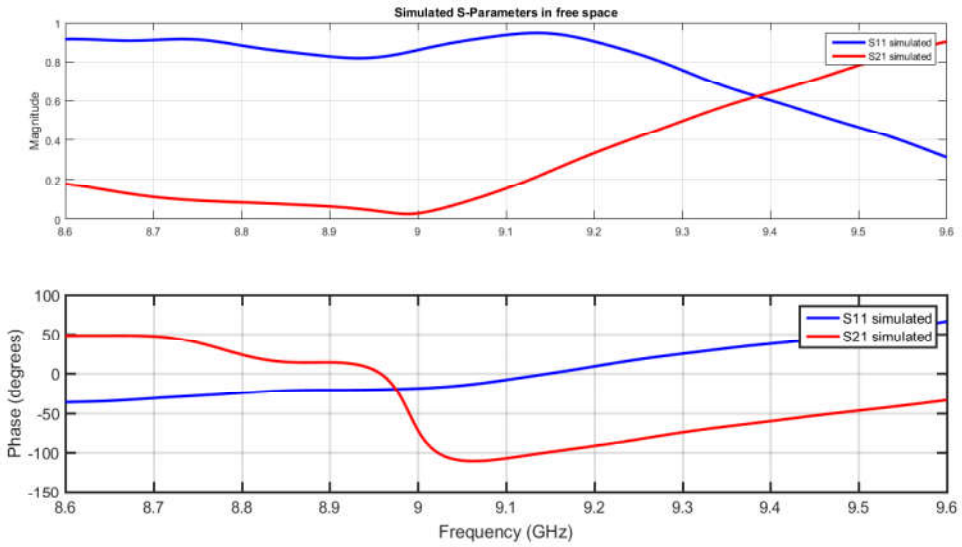

Figure 30 – Simulated S-Parameters of the metamaterial cell in free space

Based on the phase of S_{21}, the resonance frequency is found around 9.05 GHz. It is worth noticing that the magnitude of S_{11} is smaller than that observed inside the waveguide.

The relative permittivity and permeability are then retrieved using the method from Appendix A and displayed, respectively, in Figures 36 (a) and (b).

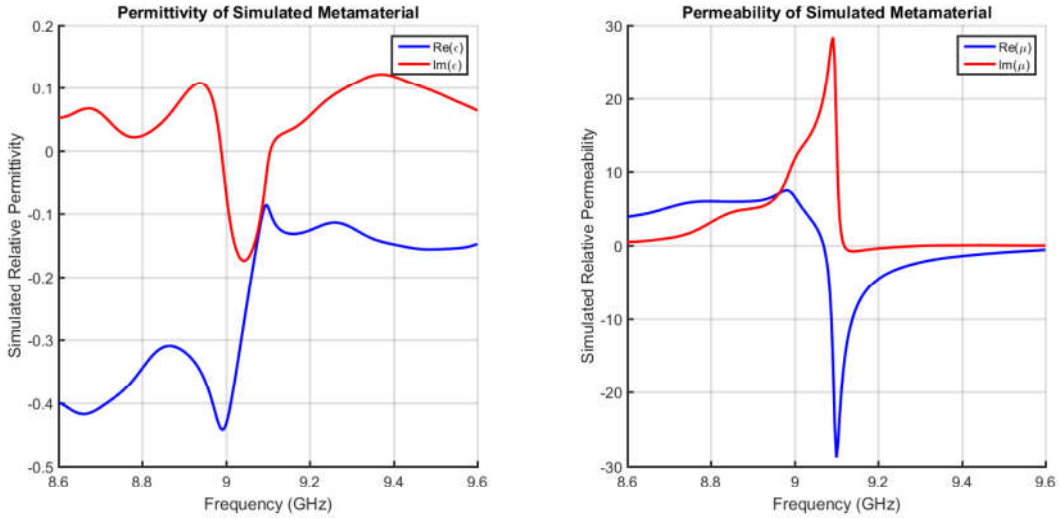

Figure 31 – Constitutive parameter obtained from simulated metamaterial inside waveguide. (a) Relative permittivity, (b) Relative permeability.

As expected, the relative permeability for the Omega-type cells is much smaller when compared to the cells used inside the waveguide which can be attributed to the array of conductors present in the latter.

The index of refraction and normalized impedance are calculated and shown in Figures 32 and 33.

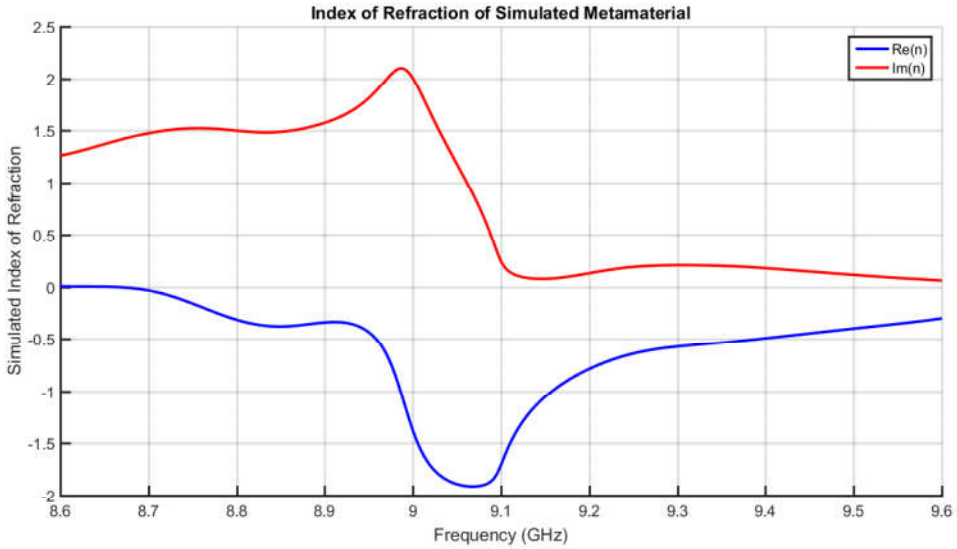

Figure 32 – Refractive index obtained from simulation of the metamaterial in free space

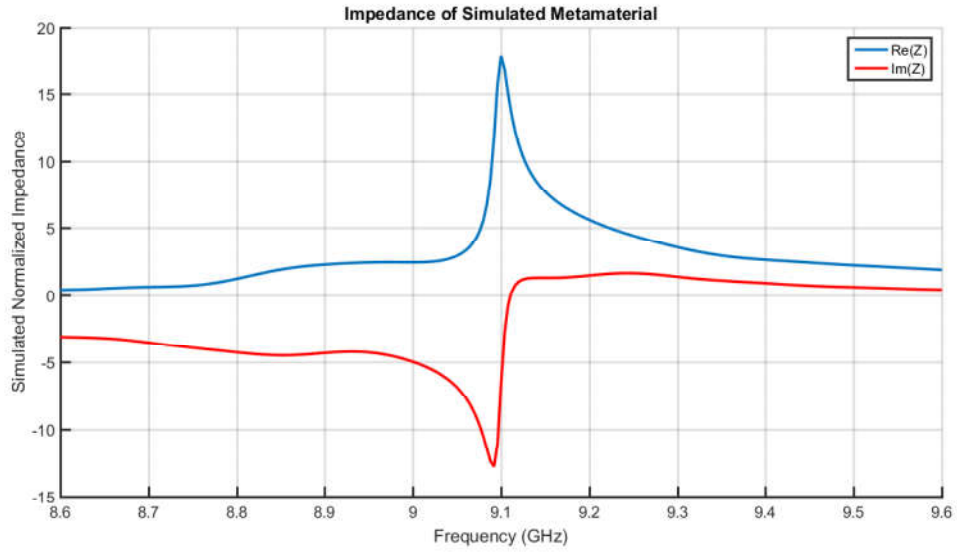

Figure 33 – Normalized impedance obtained from simulation of the metamaterial cell in free space

By analyzing Figure 32, it becomes clear that the index of refraction of the material is negative from 8.7 to 9.6 GHz, reaching a minimum of -1.9 next to the resonance frequency. Differently from the impedance of the metamaterial inside the waveguide, Figure 33 shows that the real part of the impedance also has negative values.

6.2.2 Measurements

With the designed and fabricated Omega-type metamaterials, the cells are arranged between two pyramidal antennas of 15dBi and they are connected to the Network Analyzer ZVA 40, as shown in Figure 34. The measured S-Parameters are plotted in Figure 35.

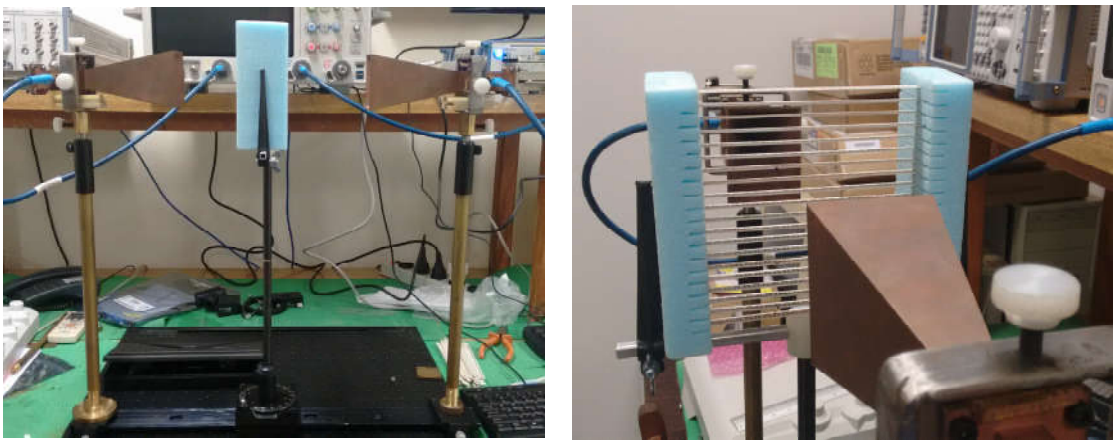

Figure 34 – Set up to measure the S-Parameters with the cells in free space. (a) View from the side, (b) View from the antenna.

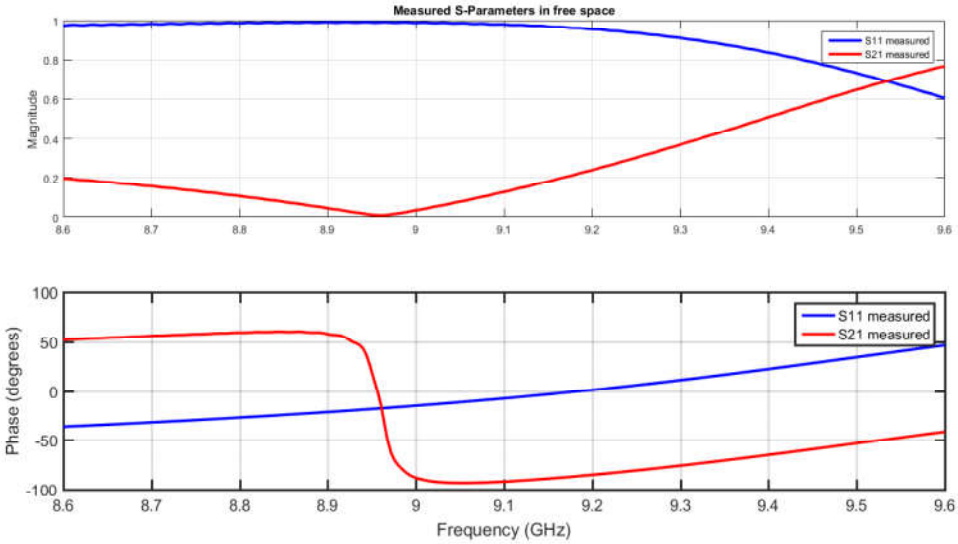

Figure 35 – Measured S-Parameters of the metamaterial cell in free space

Just like observed for the measured scattering parameters for the metamaterial inside the waveguide, the resonance frequency shows a slight shift to 9 GHz. Comparing Figures 24 with 35, it can be seen that more power is being reflected the experimental result, since S_{11} is larger.

The permittivity and permeability, index of refraction, and normalized impedance are plotted in Figures 36, 37 37, respectively. All these results show similar behavior to the simulated parameters seen, respectively, in Figures 32, 33 and 34.

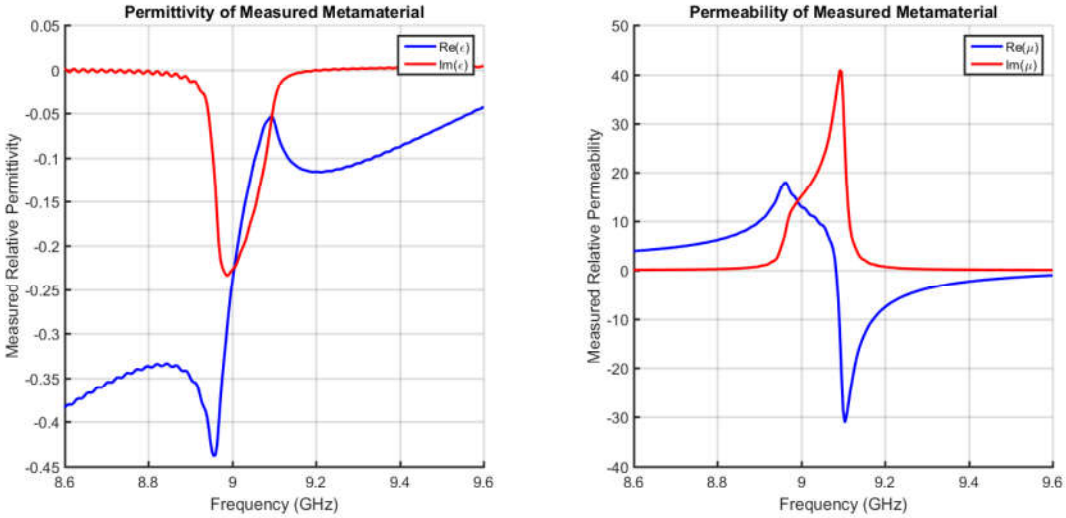

Figure 36 – Constitutive parameter obtained from measured metamaterial inside waveguide. (a) Relative permittivity, (b) Relative permeability.

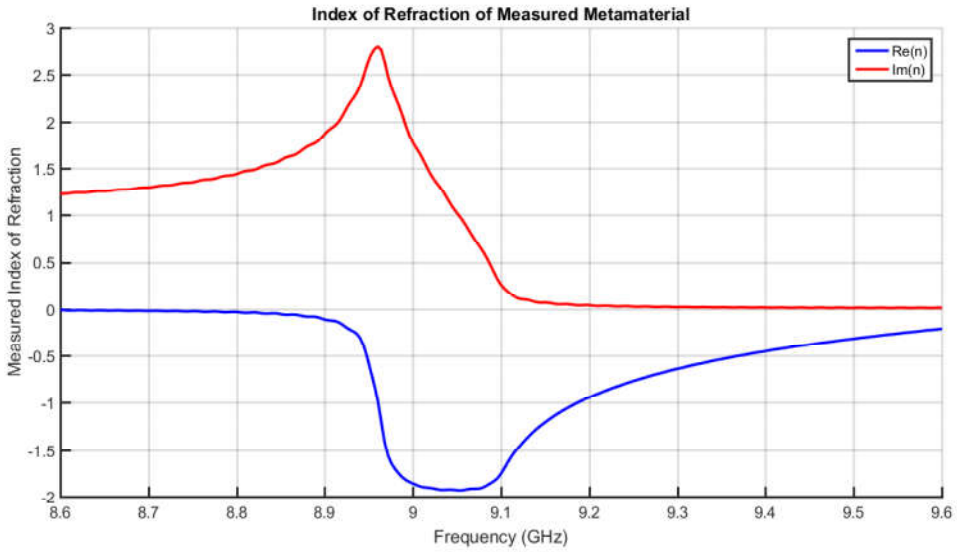

Figure 37 – Measured index of refraction of the metamaterial cell in free space

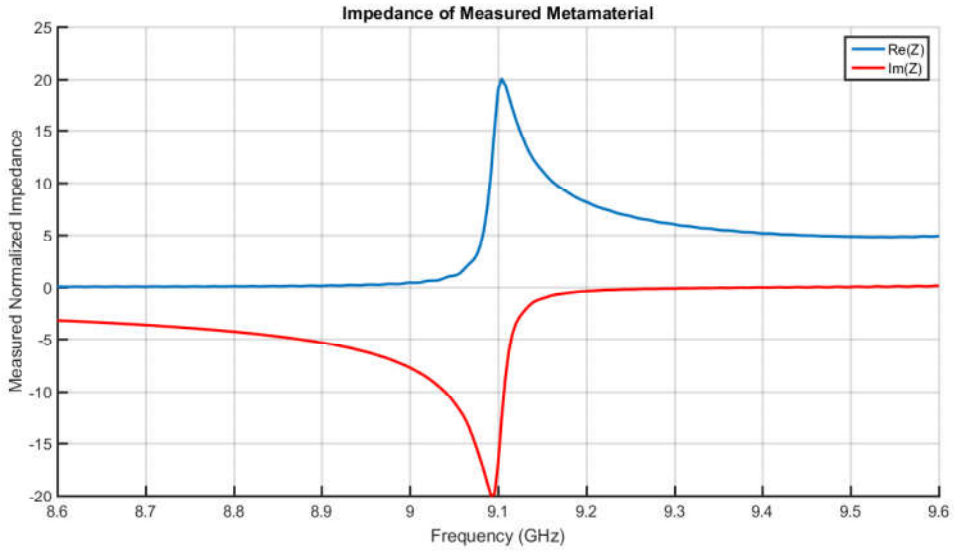

Figure 38 – Measured impedance of the metamaterial cell in free space

6.2.3 Summary

The comparison of the index of refraction of the simulated metamaterial with the measured one is plotted in Figure 39.

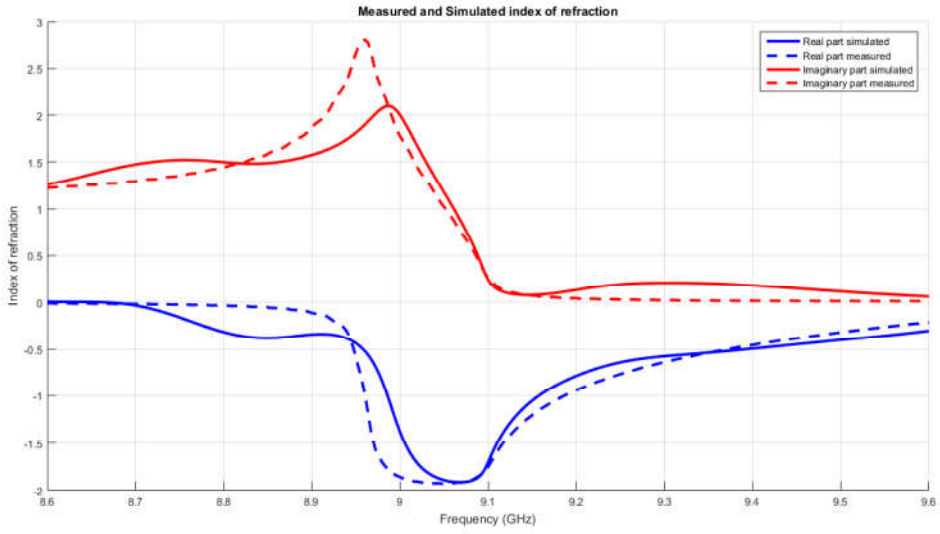

Figure 39 – Comparison between index of refraction for the simulated and measured metamaterial in free space

According to Figure 39, the index of refraction of the simulated and measured experiments have the same behavior and practically the same magnitude. Again, there is a shift on the resonance frequency, proving that the response is sensitive to geometrical variations during the fabrication/characterization procedure.

CHAPTER

7

CONCLUSION

This work covered the basic concepts of metamaterials and their properties using the effective media theory. The retrieval of electromagnetic parameters from a designed structure with negative values of refractive index was carried out via the S-Parameters of the metamaterial both in a waveguide environment and in free space.

The equations relating the S-Parameters with the permittivity and permeability were described and implemented in Matlab for each case. In addition, it was also observed that a media can be described by its index of refraction and impedance.

Two types of metamaterial's structure were chosen for measurements: an omega-type cell for free space and SRR with an array of conductors for inside a waveguide. These two types were designed with HFSS and later fabricated.

Finally, the results showed that the design of the cells was correct, since the index of refraction recovered from the measured S-Parameters had the negative real values in a frequency band. Nevertheless, the analysis also showed the extraction procedure is satisfactory and useful for the analysis of electromagnetic structures showing not only negative refraction but any behavior achievable with the metamaterial design.

For future work, it will be explored possible application for the materials fabricated. And in order to obtain better simulated results inside the waveguide, the it will be

For future work, it will be studied how to improve the simulations process to be similar to the experiment, providing data to compare the experimental results. Possible applications for the metamaterials fabricated will also be studied to ensure

BIBLIOGRAPHY

ALAM, T.; FARUQUE, M. R. I.; ISLAM, M. T. A double-negative metamaterial-inspired mobile wireless antenna for electromagnetic absorption reduction. **Materials**, Multidisciplinary Digital Publishing Institute, v. 8, n. 8, p. 4817–4828, 2015. Cited on page 8.

BALANIS, C. A. **Advanced engineering electromagnetics**. [S.l.]: John Wiley & Sons, 2012. Cited on page 13.

BARROSO, J.; HASAR, U. Constitutive parameters of a metamaterial slab retrieved by the phase unwrapping method. **Journal of Infrared, Millimeter, and Terahertz Waves**, Springer, v. 33, n. 2, p. 237–244, 2012. Cited 3 times on pages 1, 17, and 19.

BARROSO, J.; PAULA, A. D. Retrieval of permittivity and permeability of homogeneous materials from scattering parameters. **Journal of Electromagnetic Waves and Applications**, Taylor & Francis, v. 24, n. 11-12, p. 1563–1574, 2010. Cited 2 times on pages 1 and 14.

DAS, S. Metamaterials arrive in cellphones. **IEEE Spectrum, Oct**, 2009. Cited on page 8.

ERGIN, T.; STENGER, N.; BRENNER, P.; PENDRY, J. B.; WEGENER, M. Three-dimensional invisibility cloak at optical wavelengths. **Science**, American Association for the Advancement of Science, v. 328, n. 5976, p. 337–339, 2010. Cited on page 1.

GRIFFITHS, D. J.; COLLEGE, R. **Introduction to electrodynamics**. [S.l.]: prentice Hall Upper Saddle River, NJ, 1999. v. 3. Cited on page 3.

HASAR, U.; BARROSO, J.; KAYA, Y.; BUTE, M.; ERTUGRUL, M. Simple procedure for robust and accurate complex permittivity measurements of low-loss materials over a broad frequency band. **Journal of Electromagnetic Waves and Applications**, Taylor & Francis, v. 28, n. 8, p. 903–915, 2014. Cited on page 14.

JAKŠIĆ, Z.; VUKOVIĆ, S.; MATOVIC, J.; TANASKOVIĆ, D. Negative refractive index metasurfaces for enhanced biosensing. **Materials**, Molecular Diversity Preservation International, v. 4, n. 1, p. 1–36, 2010. Cited on page 8.

KITIC, G.; RADONIC, V.; CRNOJEVIC-BENGIN, V. Soil moisture sensors based on meta-materials. **Songklanakarin Journal of Science ad Technology**, v. 34, n. 6, p. 689–693, 2012. Cited on page 8.

MOTA, A. F. d. **Análise de propagação de pulso em meios metamateriais**. Tese (Doutorado) — Universidade de São Paulo, 2015. Cited on page 33.

NICOLSON, A.; ROSS, G. Measurement of the intrinsic properties of materials by time-domain techniques. **IEEE Transactions on instrumentation and measurement**, IEEE, v. 19, n. 4, p. 377–382, 1970. Cited 2 times on pages 1 and 14.

ORFANIDIS, S. J. **Electromagnetic waves and antennas**. [S.l.]: Rutgers University New Brunswick, NJ, 2002. Cited 4 times on pages 3, 6, 9, and 11.

PADILLA, W. J.; BASOV, D. N.; SMITH, D. R. Negative refractive index metamaterials. **Materials today**, Elsevier, v. 9, n. 7, p. 28–35, 2006. Cited 2 times on pages 4 and 5.

PENDRY, J.; HOLDEN, A.; STEWART, W.; YOUNGS, I. Extremely low frequency plasmons in metallic mesostructures. **Physical review letters**, APS, v. 76, n. 25, p. 4773, 1996. Cited on page 5.

PENDRY, J. B. Negative refraction makes a perfect lens. **Physical review letters**, APS, v. 85, n. 18, p. 3966, 2000. Cited 2 times on pages 7 and 8.

PENDRY, J. B.; HOLDEN, A. J.; ROBBINS, D.; STEWART, W. Magnetism from conductors and enhanced nonlinear phenomena. **IEEE transactions on microwave theory and techniques**, IEEE, v. 47, n. 11, p. 2075–2084, 1999. Cited 2 times on pages 4 and 5.

PENDRY, J. B.; SCHURIG, D.; SMITH, D. R. Controlling electromagnetic fields. **science**, American Association for the Advancement of Science, v. 312, n. 5781, p. 1780–1782, 2006. Cited on page 1.

SHAMONIN, M.; RADKOVSKAYA, O.; STEVENTS, C.; FAULKNER, G.; EDWARDS, D.; SYDORUK, O.; ZHUROMSKYY, O.; SHAMONINA, E.; SOLYMAR, L. Waveguide and sensor systems comprising metamaterial element. In: **Proceedings of the DPG—Spring Meeting of the Division Condensed Matter**. [S.l.: s.n.], 2006. p. 114–118. Cited on page 8.

SILVEIRINHA, M. G.; ENGHETA, N. Theory of supercoupling, squeezing wave energy, and field confinement in narrow channels and tight bends using ε near-zero metamaterials. **Physical Review B**, APS, v. 76, n. 24, p. 245109, 2007. Cited on page 1.

SMITH, D.; VIER, D.; KOSCHNY, T.; SOUKOULIS, C. Electromagnetic parameter retrieval from inhomogeneous metamaterials. **Physical review E**, APS, v. 71, n. 3, p. 036617, 2005. Cited 2 times on pages 2 and 4.

SMITH, D.; VIER, D.; PADILLA, W.; NEMAT-NASSER, S. C.; SCHULTZ, S. Loop-wire medium for investigating plasmons at microwave frequencies. **Applied Physics Letters**, AIP Publishing, v. 75, n. 10, p. 1425–1427, 1999. Cited on page 5.

SMITH, D. R.; PADILLA, W.; VIER, D.; SHELBY, R.; NEMAT-NASSER, S.; KROLL, N.; SCHULTZ, S. Left-handed metamaterials. In: **Photonic crystals and light localization in the 21st century**. [S.l.]: Springer, 2001. p. 351–371. Cited on page 3.

SMITH, D. R.; PADILLA, W. J.; VIER, D.; NEMAT-NASSER, S. C.; SCHULTZ, S. Composite medium with simultaneously negative permeability and permittivity. **Physical review letters**, APS, v. 84, n. 18, p. 4184, 2000. Cited on page 4.

ZHANG, F.; HOUZET, G.; LHEURETTE, E.; LIPPENS, D.; CHAUBET, M.; ZHAO, X. Negative-zero-positive metamaterial with omega-type metal inclusions. **Journal of Applied Physics**, AIP Publishing, v. 103, n. 8, p. 084312, 2008. Cited 2 times on pages 2 and 21.

ZIOLKOWSKI, R. W.; KIPPLE, A. D. Application of double negative materials to increase the power radiated by electrically small antennas. **IEEE Transactions on Antennas and Propagation**, IEEE, v. 51, n. 10, p. 2626–2640, 2003. Cited 2 times on pages 6 and 8.

APPENDIX

A

PARAMETER EXTRACTION INSIDE THE WAVEGUIDE

```
function [eps,mu,n,Z] = extraction_waveguide(S11,S21,f,sample_width,
    n_pi)

  global a eps0 mu0;

  omega = 2*pi*f;
  lamc = 2*a;
  fc = 3e8/lamc;

  lam0 = 3e8./f;
  lamg = lam0./sqrt(1-(lam0./lamc).^2);

  K=(S11.^2-S21.^2+1)./(2*S11);
  ref=zeros(max(size(S11)),1);
  for i=1:size(S11,1)
    ref(i)=K(i)+sqrt(K(i)^2-1);
    if abs(ref(i))>=1
      ref(i)=K(i)-sqrt(K(i)^2-1);
    end
  end
  T1=(S11+S21-ref)./(1-(S21+S11).*ref);
  Z = (1+ref)./(1-ref);

  for i=1:max(size(Z))
    if real(Z(i))<=0
      Z(i) = -Z(i);
```

```
26      end
27    end
28
29    T=1/(2*pi*sample_width).*(1i*log(abs(T1))-angle(T1)-2*n_pi*pi);
30
31    mu = lamg.*T.*Z;
32    eps = lam0.^2.*((T.^2) + lamc.^(-2))./mu;
33
34
35    n =sqrt(mu.*eps);
36      for i=1:max(size(T))
37        if imag(n(i))<=0
38          n(i) = -(n(i));
39        end
40      end
41    end
42  end
```

APPENDIX

B

PARAMETER EXTRACTION IN FREE SPACE

```
function [eps, mu, n, Z] = extraction_free_space(S11, S21, f,
    sample_width, N, n_pi)

  k=2*pi*f/3e8;
  K=(S11.^2-S21.^2+1)./(2*S11);
  ref(1:size(S11),1)=0;
  for a=1:size(S11)
     ref(a)=K(a)+sqrt(K(a)^2-1);
     if abs(ref(a,1))>=1
        ref(a)=K(a)-sqrt(K(a)^2-1);
     end
  end

  T1=S21./(1-S11.*ref);
  T=1/(2*pi*sample_width).*(-1i*log(abs(T1))+angle(T1)+2*pi*n_pi);
  mu=(2*pi./k).*T.*((1+ref)./(1-ref));
  eps=(2*pi./k).^2.*(T.^2)./(mu);
  n=zeros(size(S11,1),1);
  Z=zeros(size(S11,1),1);

  for a=1:size(S11)

     n(a)=sqrt(mu(a)*eps(a));
     if(imag(n(a))<0)
        n(a)=-sqrt(mu(a)*eps(a));
     end

     Z(a)=sqrt(mu(a)/eps(a));
```

```
28        if(real(Z(a))<0)
29          Z(a)=-Z(a);
30        end
31      end
32
33  end
```